Supporting Information

Inter- and Intra-Molecular Electron-Transfer Reduction Properties of Coronenediimide Derivatives via Photoinduced Processes

Motoki Yoshida,[†] *Hayato Sakai,*[†] *Kei Ohkubo,*[‡] *Shunichi Fukuzumi,*[*§,‖] *and Taku Hasobe*[*†]

[†]Department of Chemistry, Faculty of Science and Technology, Keio University, Yokohama, 223-8522, Japan

[‡]Institute for Advanced Co-Creation Studies, Open and Transdisciplinary Research Initiatives, Osaka University, 2-1 Yamada-oka, Suita, Osaka, 565-0871, Japan

[§]Department of Chemistry and Nano Science, Ewha Womans University, Seoul 120-750, Korea

[‖]Faculty of Science and Engineering, Meijo University, SENTAN, Japan Science and Technology Agency (JST), Nagoya, Aichi 468-0073, Japan

Experimental Section

Electrochemical Measurements

Cyclic voltammograms were recorded on Iviumstat 20 V / 2.5 A potentiostat by using a three electrode system. A platinum electrode was used as the working electrode. A platinum wire served as the counter electrode, and a saturated calomel electrode was used as the reference electrode. Ferrocene/ferrocenium redox couple was used as an internal standard. All the solutions were purged prior to electrochemical and spectral measurements by using nitrogen gas.

Steady-State Spectroscopic Measurements

UV/Vis absorption spectra were recorded on Parkin Elmer (Lamda 750) UV-VIS-NIR spectrophotometer. Fluorescence emission spectra were recorded on Parkin Elmer (LS-55) spectrofluorophotometer. The absolute fluorescence quantum yields were measured by a Hamamatsu Photonics C9920-02 system equipped with an integrating sphere and a red-sensitive multichannel photodetector (PMA-12): excitation wavelength = 510 nm.

Nanosecond Time-Resolved Measurements

Nanosecond transient absorption measurements were carried out using a Unisoku TSP-2000 flash spectrometer. A Surelite-I Nd-YAG (Continuum, 4–6 ns fwhm) laser with the second harmonic at 532 nm was employed for the flash photo-irradiation exposure to a xenon lamp (150 W) as a probe light and a photomultiplier tube (Hamamatsu R-2949) as a detector. Each sample solution was purged with Ar for at least 20 min prior to the measurement. All experiments were performed at room temperature.

Femtosecond Laser Flash Photolysis

Femtosecond transient absorption spectroscopy experiments were conducted using an ultrafast source: Integra-C (Quantronix Corp.), an optical parametric amplifier: TOPAS (Light Conversion Ltd.) and a commercially available optical detection system: Helios provided by Ultrafast Systems LLC. The source for the pump and probe pulses were derived from the fundamental output of Integra-C (λ = 786 nm, 2 mJ/pulse and fwhm = 130 fs) at a repetition rate

of 1 kHz. 75% of the fundamental output of the laser was introduced into a second harmonic generation (SHG) unit: Apollo (Ultrafast Systems) for excitation light generation at λ = 393 nm, while the rest of the output was used for white light generation. The laser pulse was focused on a sapphire plate of 3 mm thickness and then white light continuum covering the visible region from λ = 410 nm to 800 nm was generated via self-phase modulation. A variable neutral density filter, an optical aperture, and a pair of polarizer were inserted in the path in order to generate stable white light continuum. Prior to generating the probe continuum, the laser pulse was fed to a delay line that provides an experimental time window of 3.2 ns with a maximum step resolution of 7 fs. In our experiments, a wavelength at λ = 393 nm of SHG output was irradiated at the sample cell with a spot size of 1 mm diameter where it was merged with the white probe pulse in a close angle (< 10°). The probe beam after passing through the 2 mm sample cell was focused on a fibre optic cable that was connected to a CMOS spectrograph for recording the time-resolved spectra (λ = 410 - 1600 nm). Typically, 1500 excitation pulses were averaged for 3 seconds to obtain the transient spectrum at a set delay time. Kinetic traces at appropriate wavelengths were assembled from the time-resolved spectral data. All measurements were conducted at room temperature.

ESR Measurements

ESR spectra were taken on a JEOL X-band spectrometer (JES-RE1XE). ESR spectra of the radical anions in deaerated CH_2Cl_2 were measured under photoirradiation with a high-pressure mercury lamp (USH–1005D) through a water filter focusing at the sample cell in the ESR cavity at 298 K. The *g* value was calibrated using an Mn^{2+} marker. The radical anions were generated by the photoinduced electron-transfer reduction of the coronenediimide derivatives (2.0×10^{-4} M) with dimeric 1-benzyl-1,4-dihydronicotinamide [$(BNA)_2$] (1.0×10^{-4}). The resulting solution was transferred to a quartz ESR tube under an atmospheric pressure of Ar. The hyperfine coupling constants were determined using the Win-Sim program of the NIEHS public ESR software tools package, which is available on the Internet (http://EPR.niehs.nih.gov/). This program was allowed to systematically vary the hydrogen and nitrogen hyperfine coupling constants and the relative concentrations of each species to achieve the best fit to the experimental spectra. The ESR spectra were recorded under non-saturating microwave power

conditions. The magnitude of modulation was chosen to optimize the resolution and the signal-to-noise (*S*/*N*) ratio of the observed spectra.

Theoretical Calculations

Density functional theory (DFT) calculations were performed with Gaussian09 (Revision C.02, Gaussian, Inc.). The calculations were performed on a 16-processor high performance computer (ForScientist XD1, HPC Systems Inc., Japan).

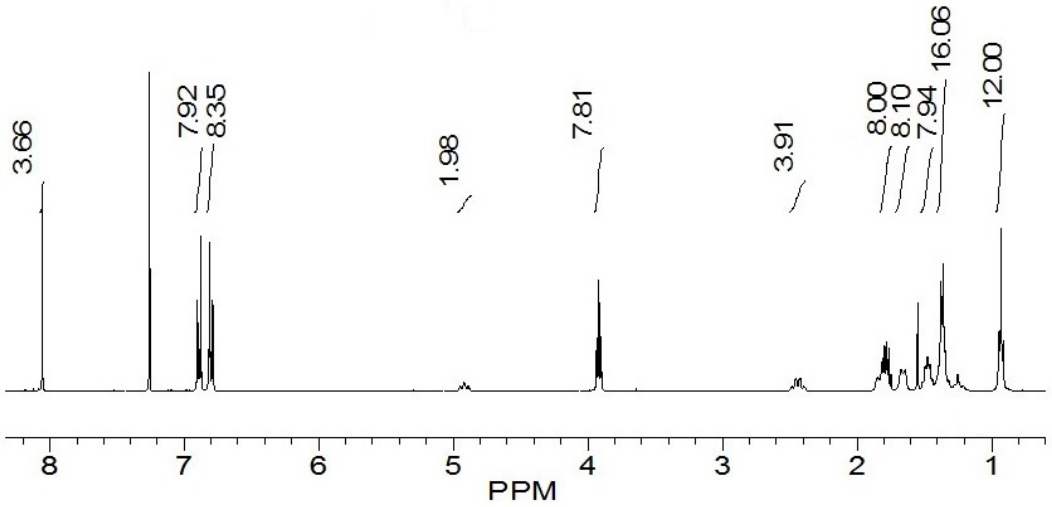

Figure S1. ^{1}H NMR spectrum of compound **2**.

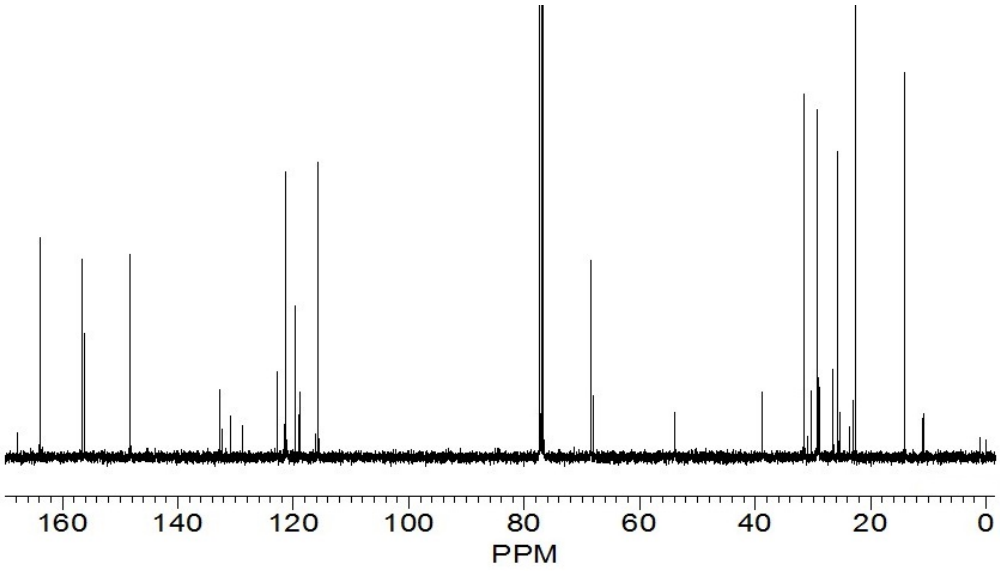

Figure S2. ^{13}C NMR spectrum of compound **2**.

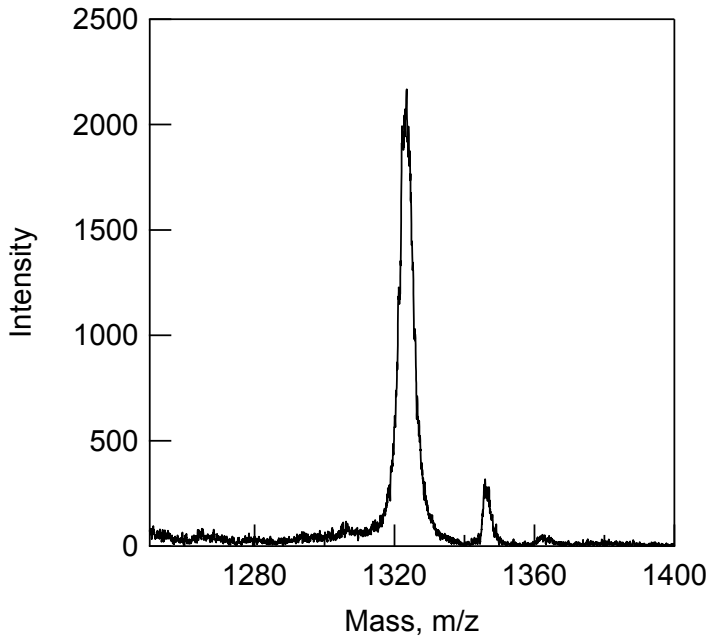

Figure S3. MALDI-TOF MS spectral profile of compound **2**.

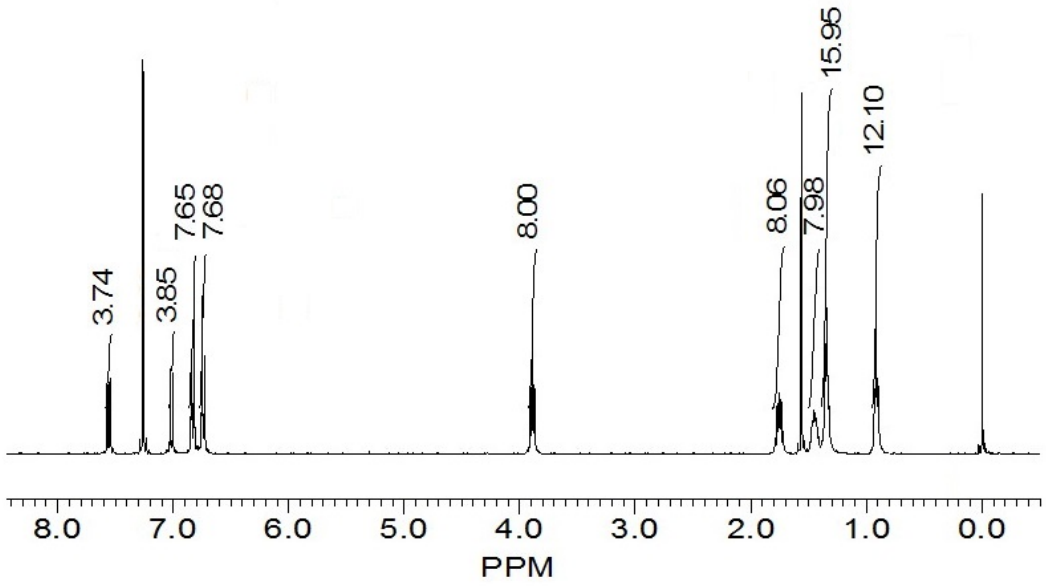

Figure S4. ^{1}H NMR spectrum of compound **4**.

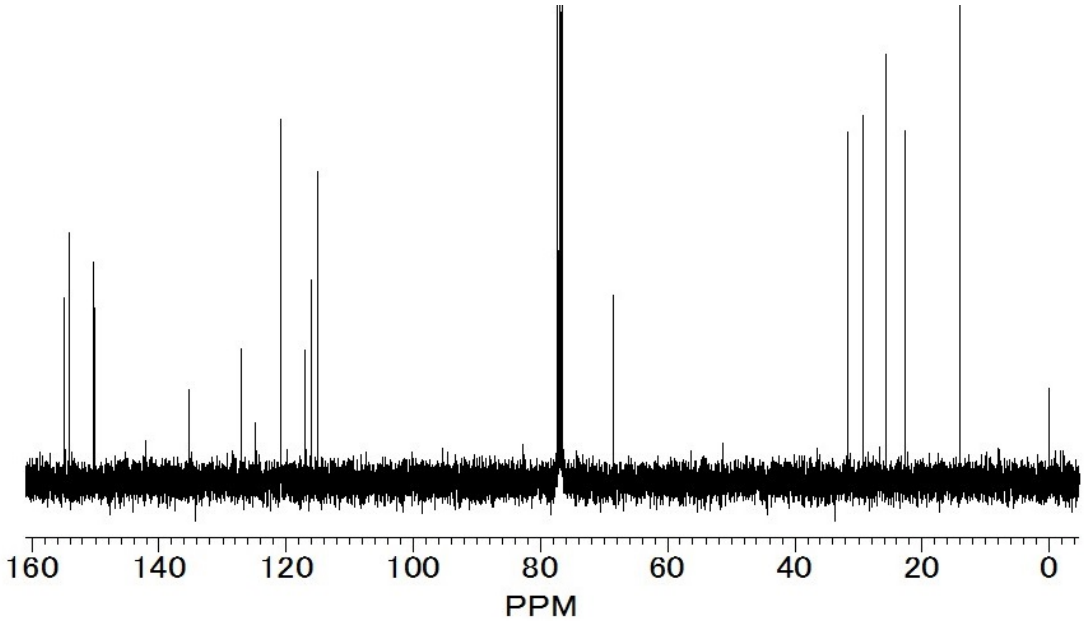

Figure S5. ^{13}C NMR spectrum of compound **4**.

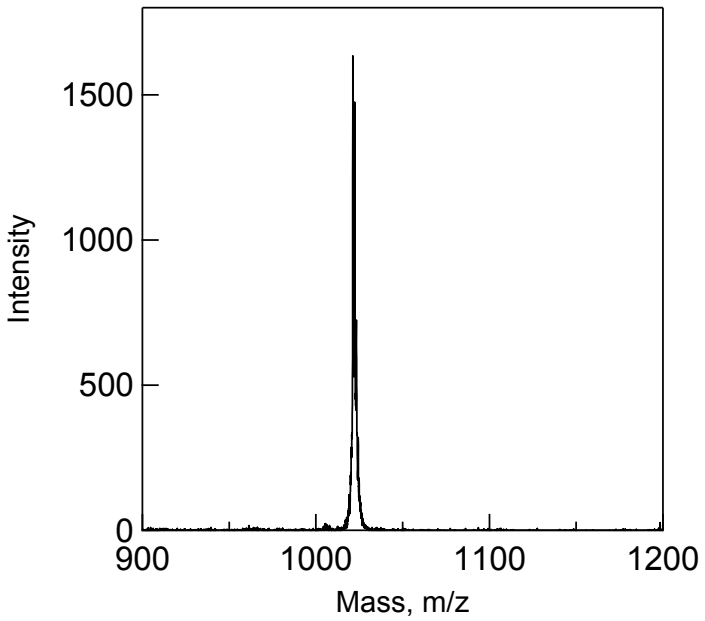

Figure S6. MALDI-TOF MS spectral profile of compound **4**.

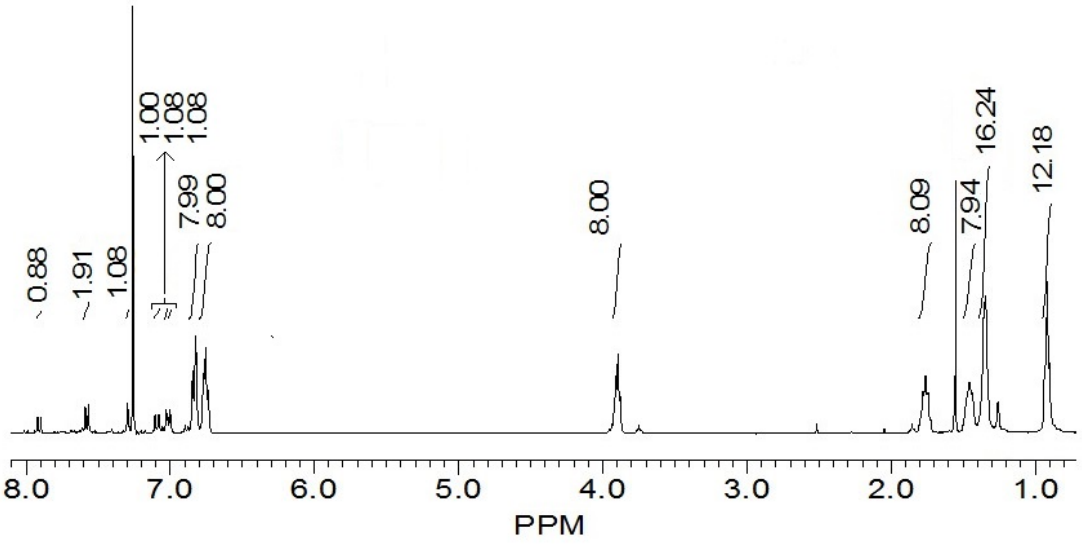

Figure S7. ^{1}H NMR spectrum of compound **5**.

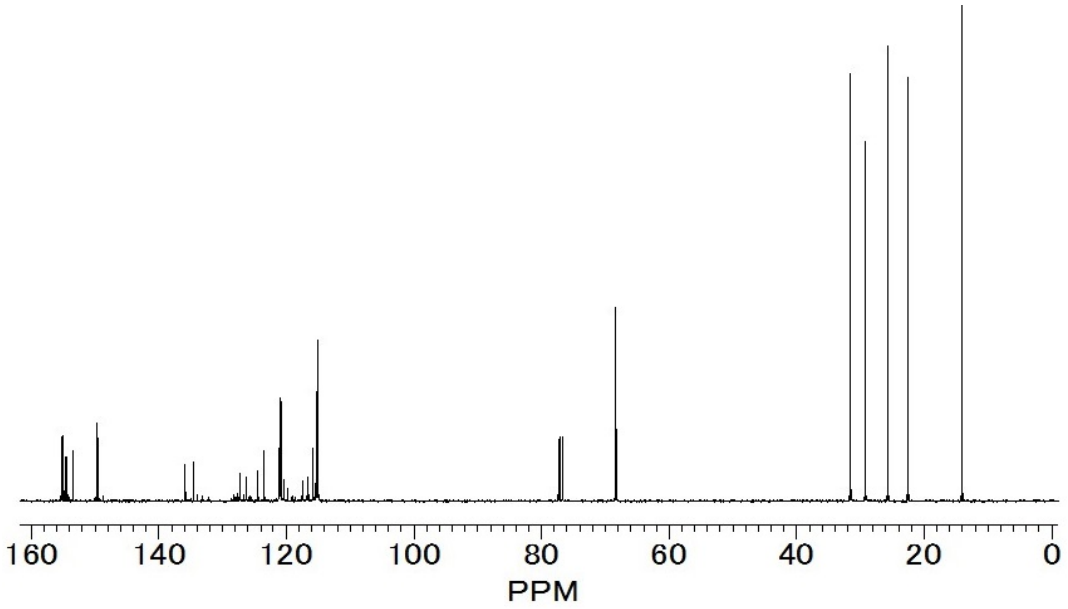

Figure S8. ^{13}C NMR spectrum of compound **5**.

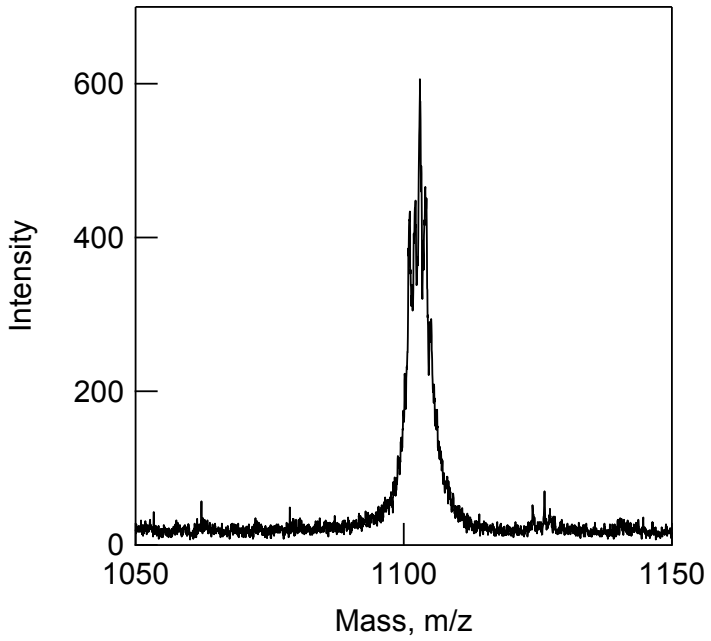

Figure S9. MALDI-TOF MS spectral profile of compound **5**.

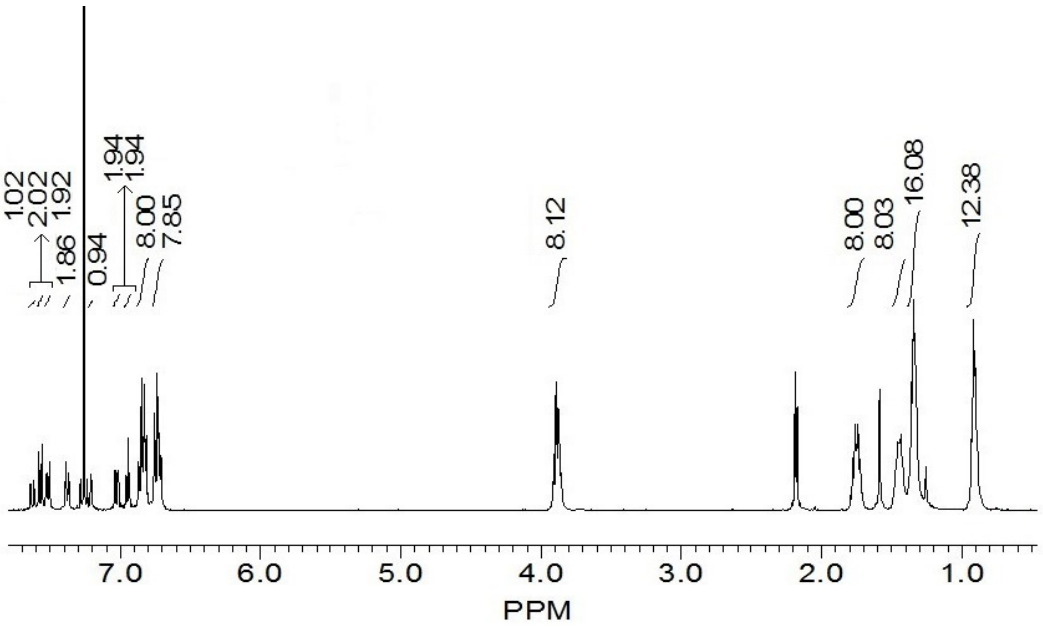

Figure S10. ^{1}H NMR spectrum of Pery.

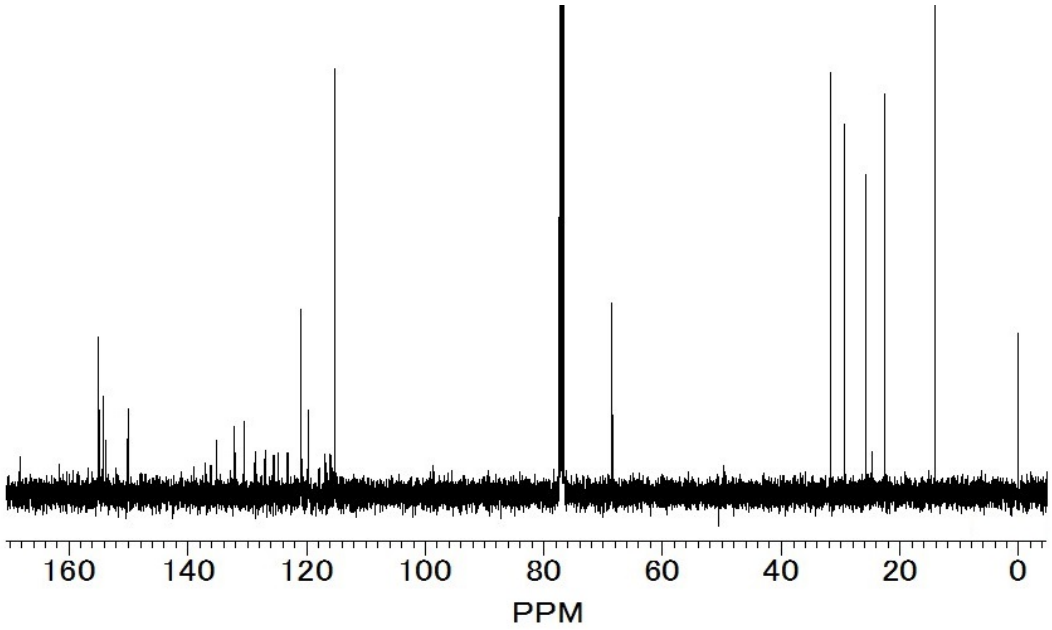

Figure S11. ^{13}C NMR spectrum of Pery.

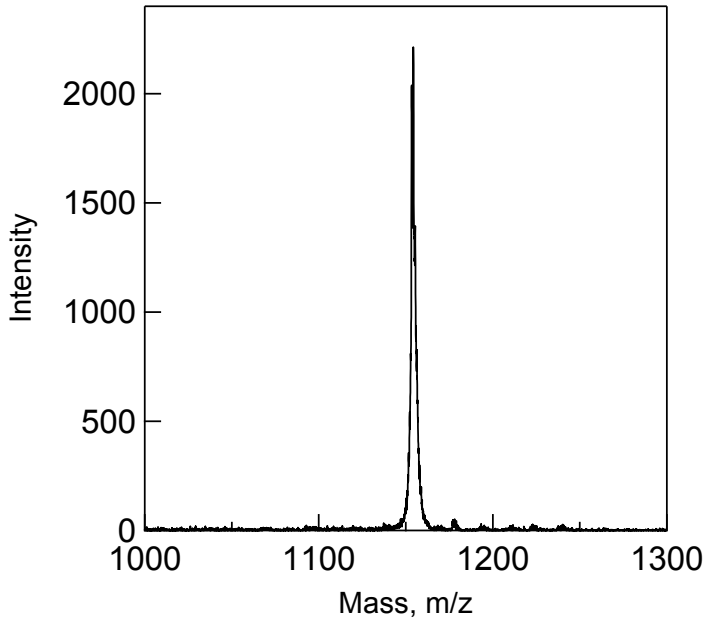

Figure S12. MALDI-TOF MS spectral profile of Pery.

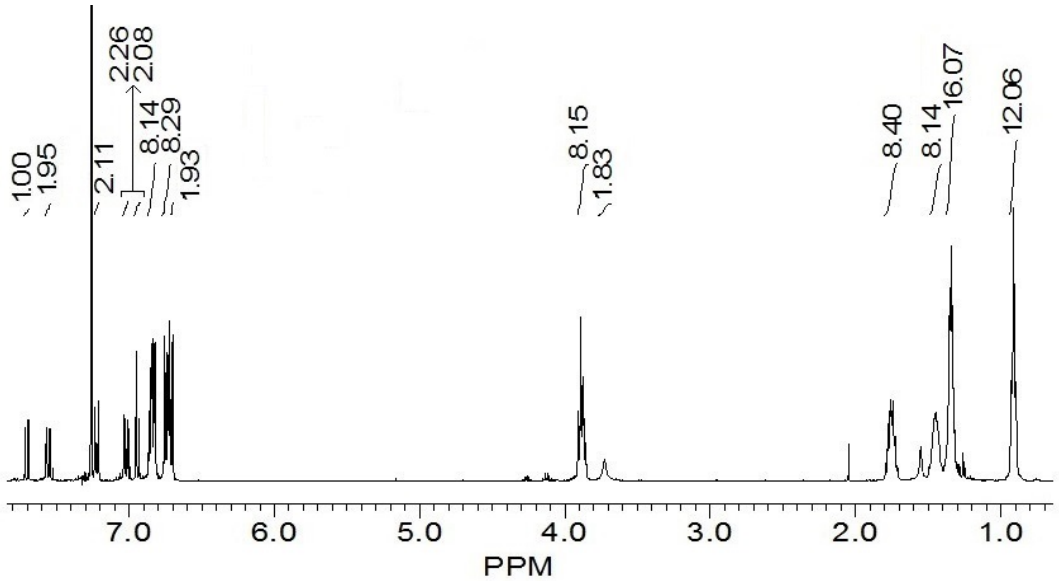

Figure S13. [1]H NMR spectrum of compound **6**.

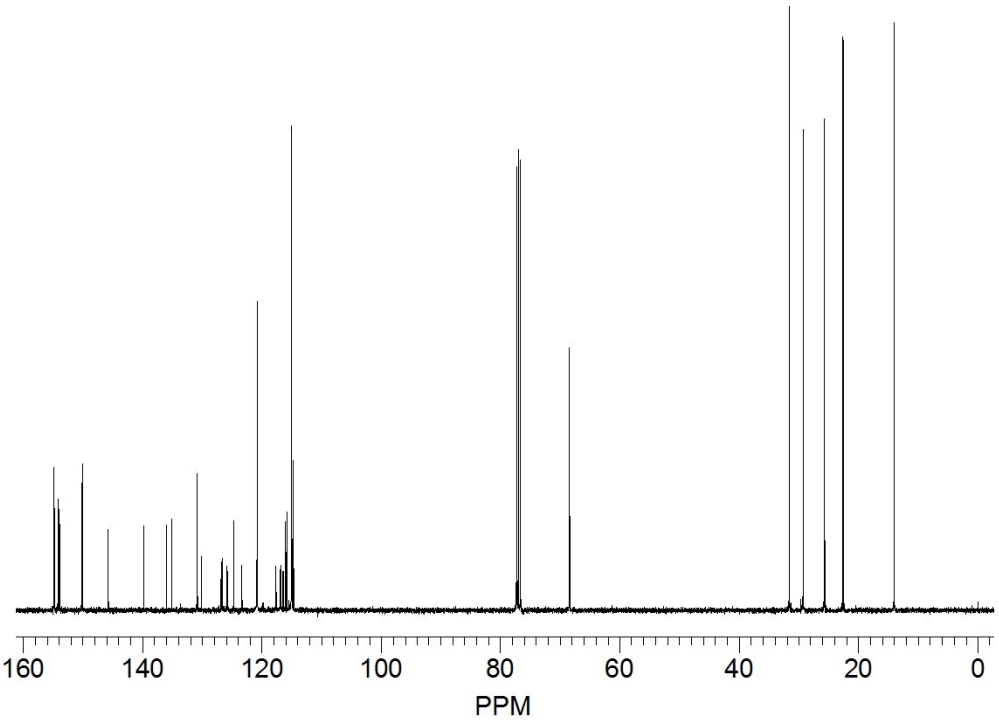

Figure S14. ^{13}C NMR spectrum of compound **6**.

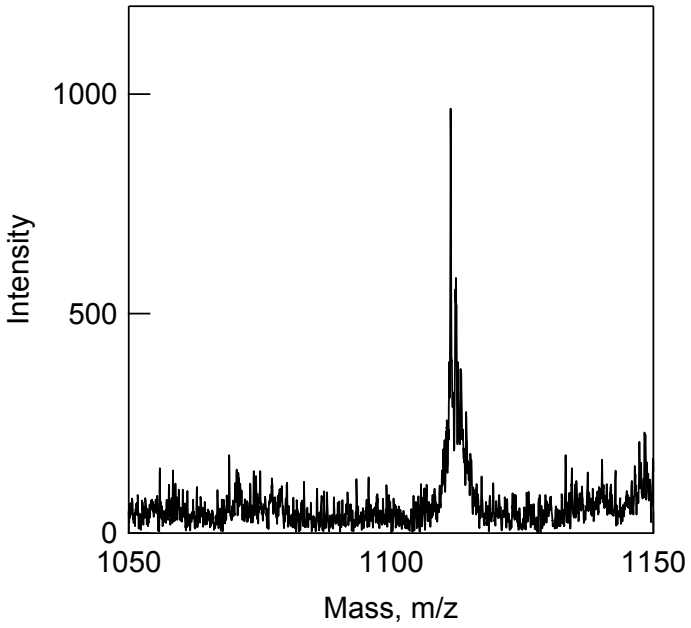

Figure S15. MALDI-TOF MS spectral profile of compound **6**.

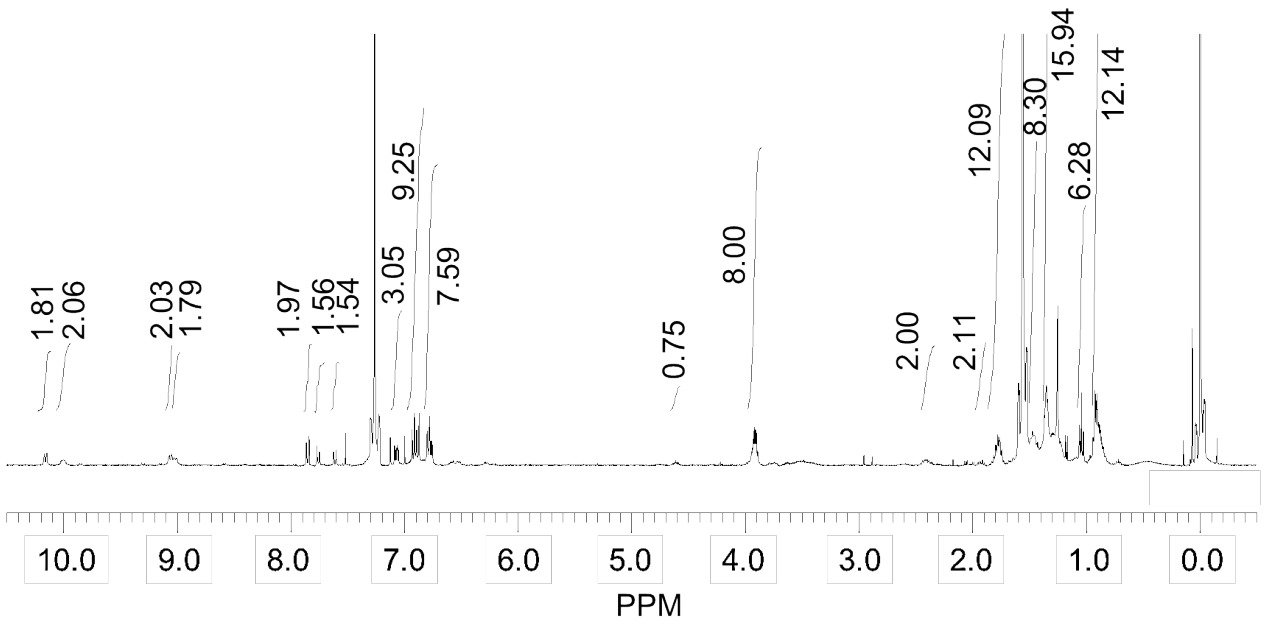

Figure S16. ^{1}H NMR spectrum Cor(5Im)$_2$-Pery.

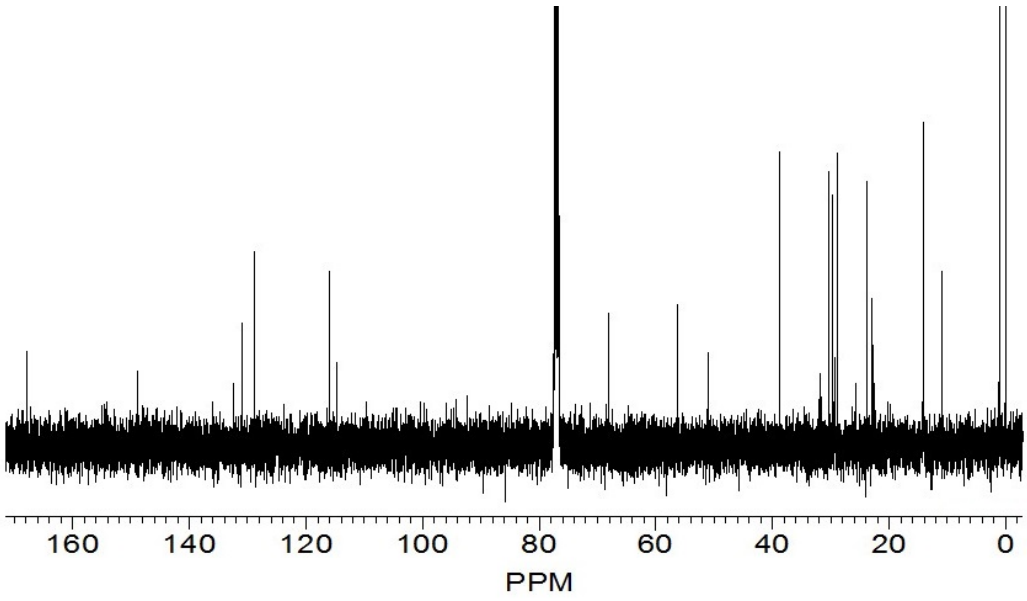

Figure S17. ^{13}C NMR spectrum of Cor(5Im)$_2$-Pery.

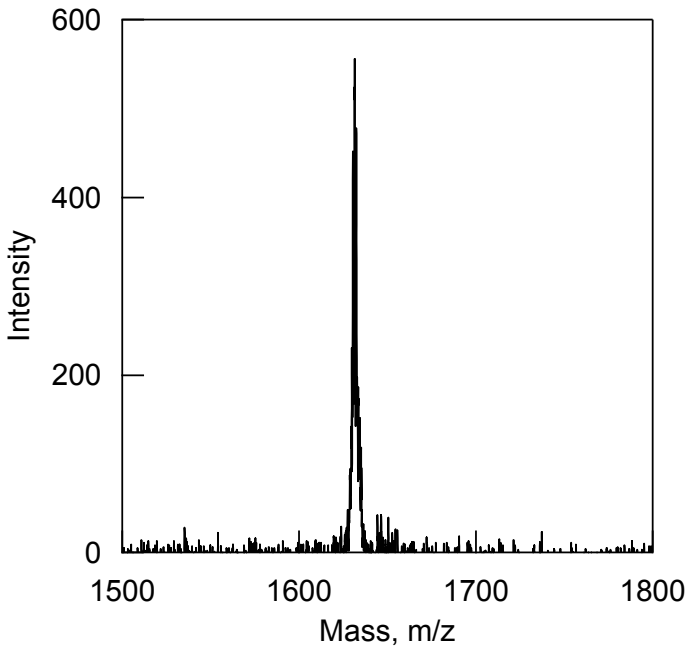

Figure S18. MALDI-TOF MS spectral profile of Cor(5Im)$_2$-Pery.

Compound	HOMO	LUMO
$Cor(5Im)_2$	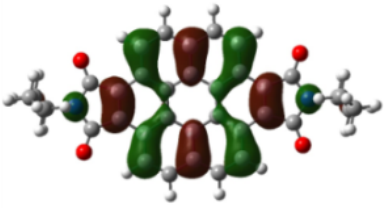	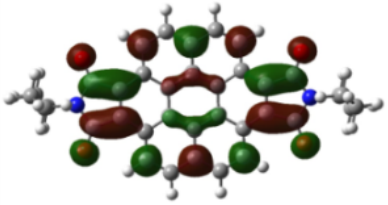
$Cor(6Im)_2$	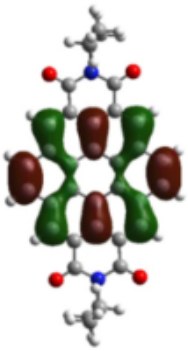	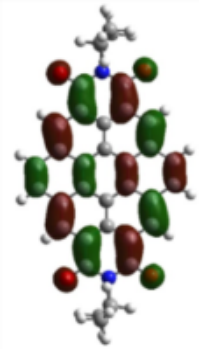
Pery	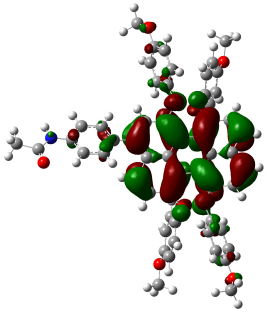	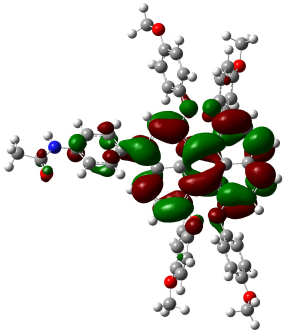
$Cor(5Im)_2$-Pery	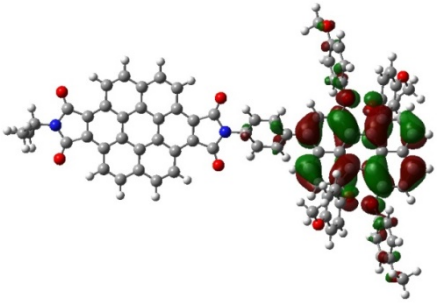	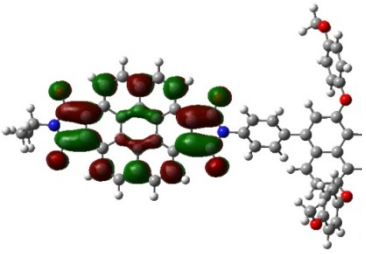

Figure S19. Molecular orbitals of $Cor(5Im)_2$, $Cor(6Im)_2$, Pery, and $Cor(5Im)_2$-Pery (calculated at B3LYP/ 6-31G(d) level of theory). The alkyl chains are omitted for clarity.

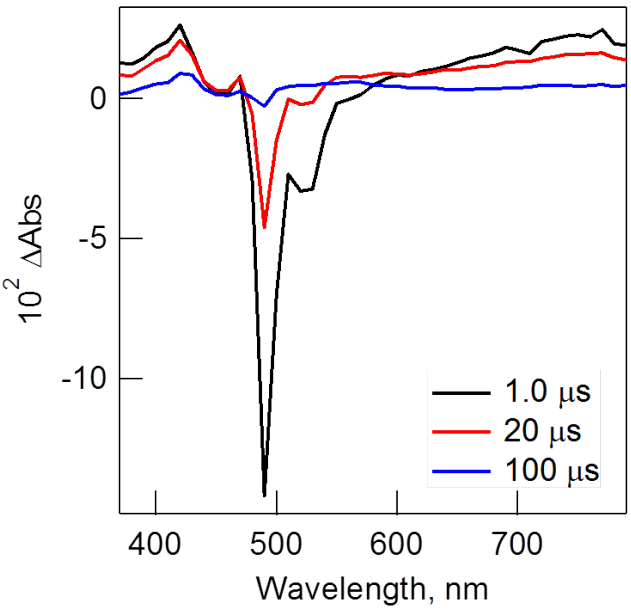

Figure S20. Transient absorption spectra of $Cor(5Im)_2$ (63 μM) in the presence of 2MI (2.2 mM) in Ar-Saturated PhCN taken at 1.0 μs (black), 20 μs (red), and 100 μs (blue) after laser excitation at 355 nm at 298 K.

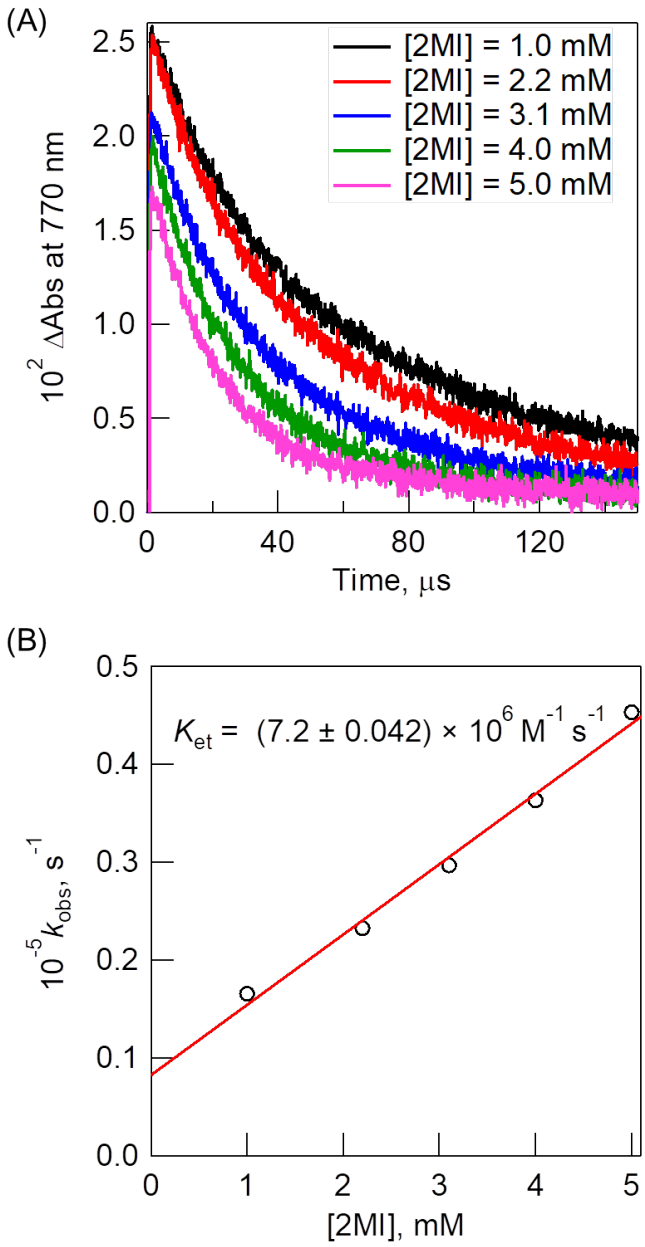

Figure S21. (A) Time profiles of absorbance at 770 nm due to $^{3}Cor(5Im)_2^{*}$ upon nanosecond laser excitation to $Cor(5Im)_2$ (55 μM) in the presence of varying concentrations of 2MI in Ar-Saturated PhCN at 298 K. (B) Plot of the pseudo-first-order rate constant (k_{obs}) vs the concentration of 2MI.

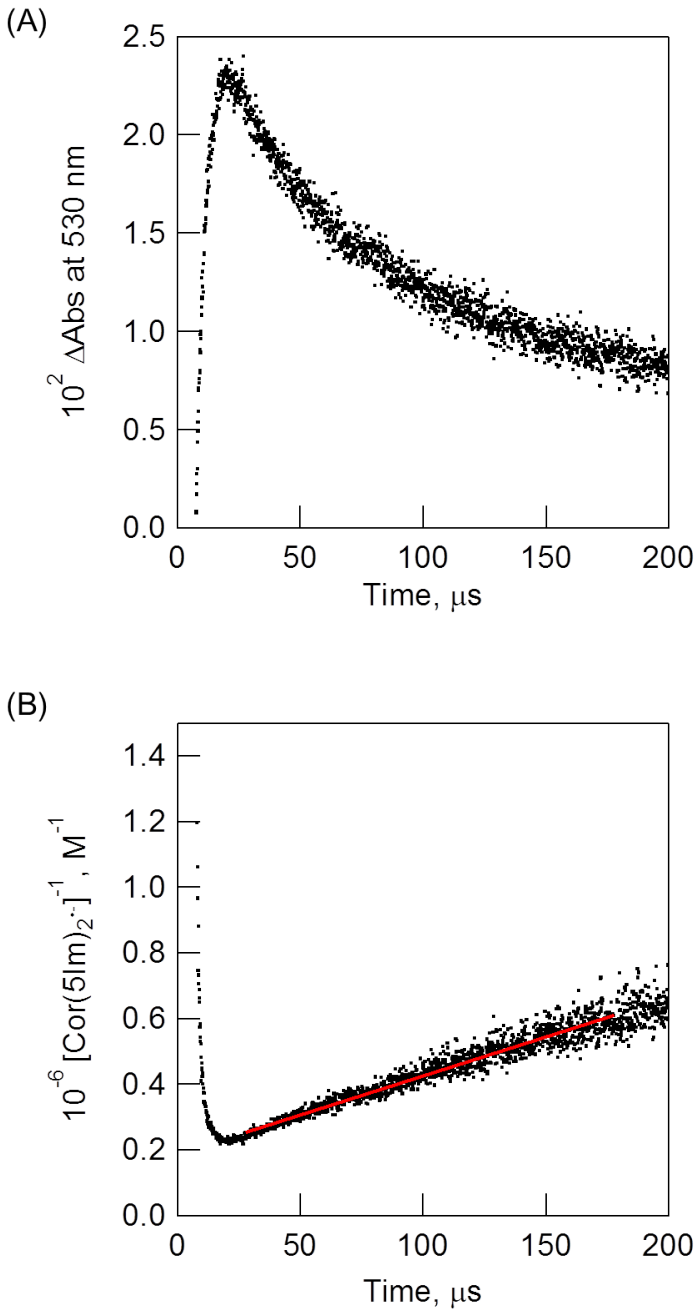

Figure S22. (A) Time profile of absorbance at 530 nm due to $Cor(5Im)_2^{\bullet-}$ upon nanosecond laser excitation to $Cor(5Im)_2$ (100 μM) and 2MI (10 mM) in Ar-Saturated PhCN at 298 K. (B) The second-order plot of the decay of $Cor(5Im)_2^{\bullet-}$ obtained from the absorbance at 530 nm and the molar absorption coefficient ($\varepsilon = 5.2 \times 10^3$ M^{-1} cm^{-1}).

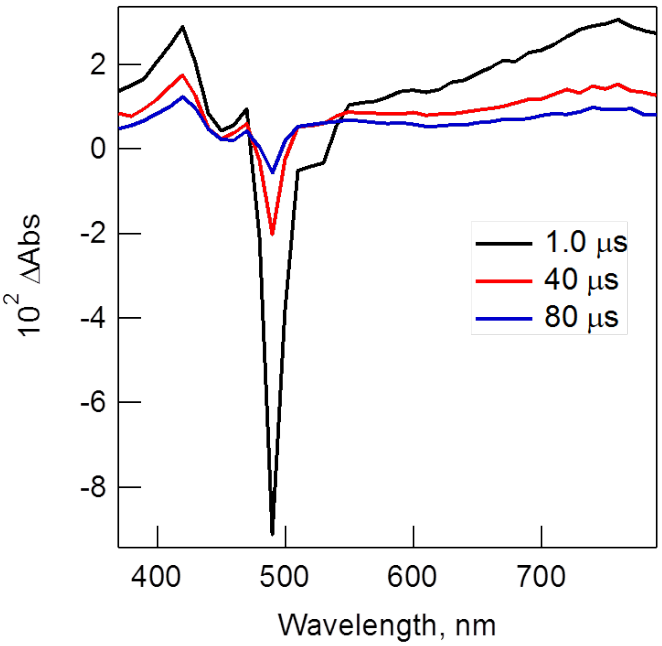

Figure S23. Transient absorption spectra of $Cor(5Im)_2$ (60 μM) in the presence of TEA (40 μM) in Ar-Saturated PhCN taken at 1.0 μs (black), 40 μs (red), and 80 μs (blue) after laser excitation at 355 nm at 298 K.

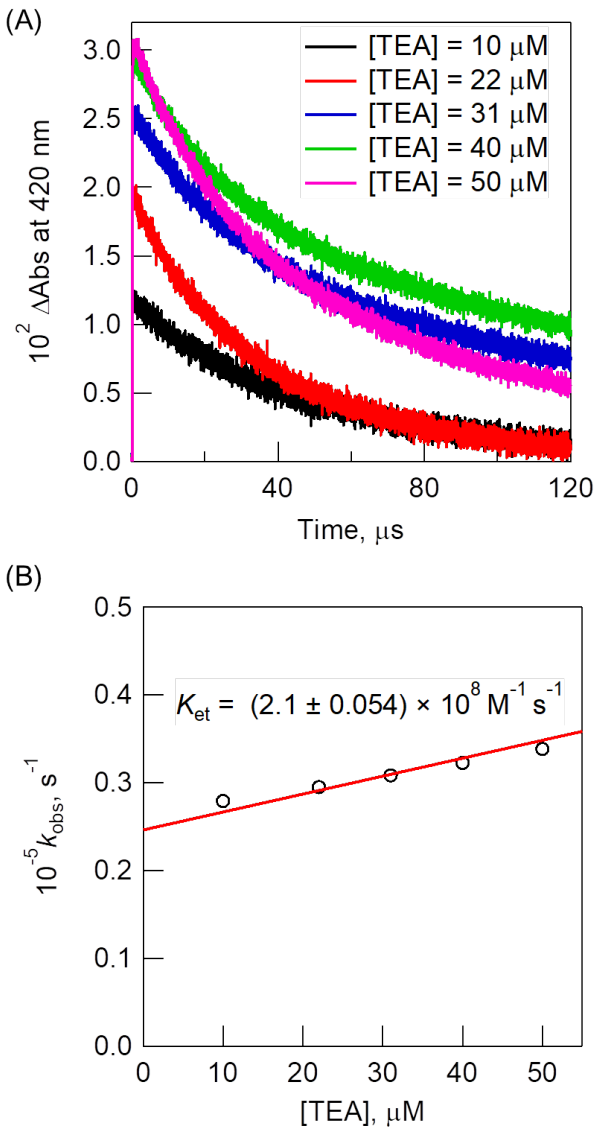

Figure S24. (A) Time profiles of absorbance at 420 nm due to $^{3}Cor(5Im)_2^{*}$ upon nanosecond laser excitation to $Cor(5Im)_2$ (69 μM) in the presence of varying concentrations of TEA in Ar-Saturated PhCN at 298 K. (B) Plot of the pseudo-first-order rate constant (k_{obs}) vs the concentration of TEA.

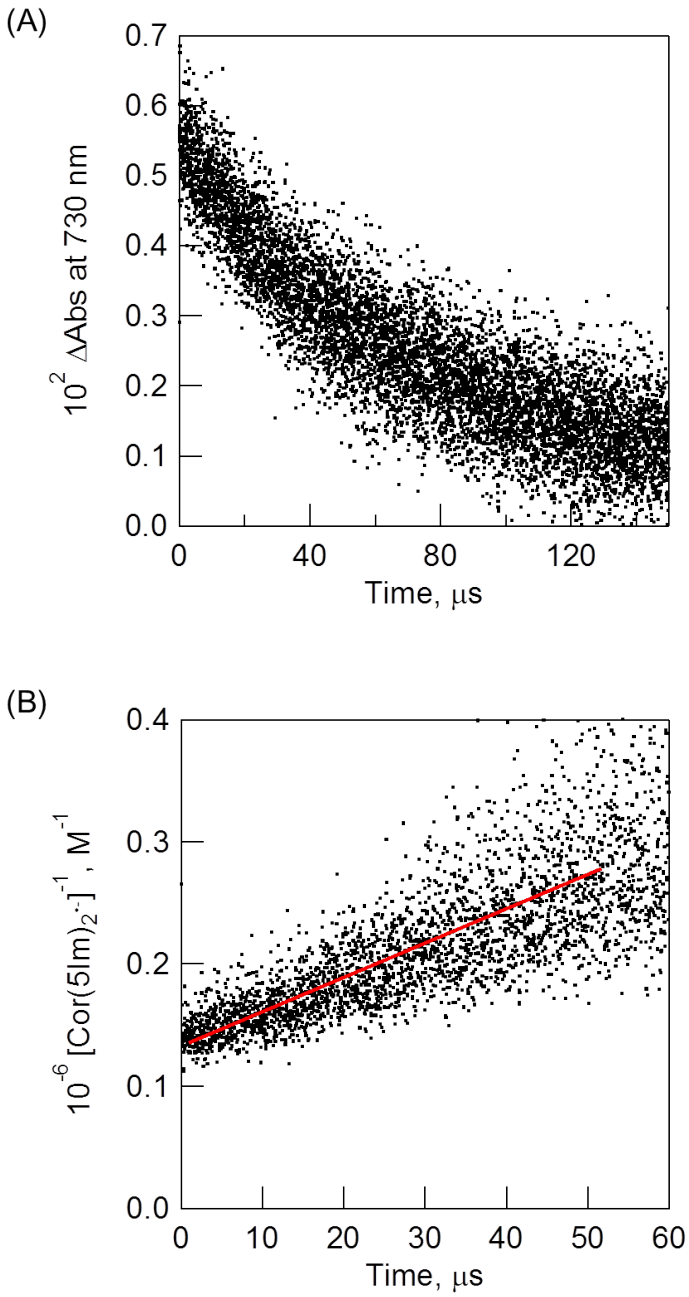

Figure S25. (A) Time profile of absorbance at 730 nm due to $Cor(5Im)_2^{\bullet-}$ upon nanosecond laser excitation to $Cor(5Im)_2$ (57 μM) and TEA (426 μM) in Ar-Saturated PhCN at 298 K. (B) The second-order plot of the decay of $Cor(5Im)_2^{\bullet-}$ obtained from the absorbance at 730 nm and the molar absorption coefficient ($\varepsilon = 7.7 \times 10^2$ M^{-1} cm^{-1}).

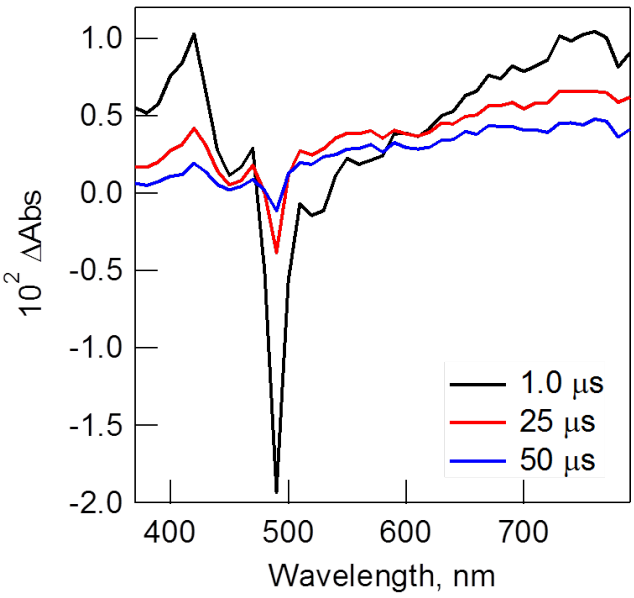

Figure S26. Transient absorption spectra of $Cor(5Im)_2$ (46 μM) in the presence of TPA (40 μM) in Ar-Saturated PhCN taken at 1.0 μs (black), 25 μs (red), and 50 μs (blue) after laser excitation at 355 nm at 298 K.

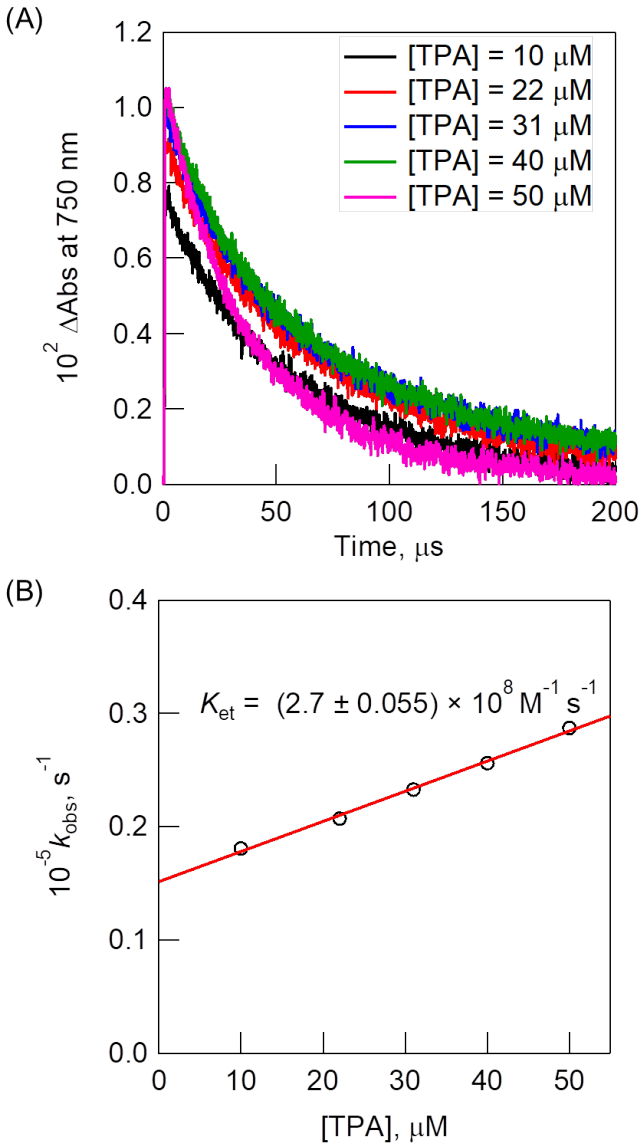

Figure S27. (A) Time profiles of absorbance at 750 nm due to $^{3}Cor(5Im)_2^{*}$ upon nanosecond laser excitation to $Cor(5Im)_2$ (53 μM) in the presence of varying concentrations of TPA in Ar-Saturated PhCN at 298 K. (B) Plot of the pseudo-first-order rate constant (k_{obs}) vs the concentration of TPA.

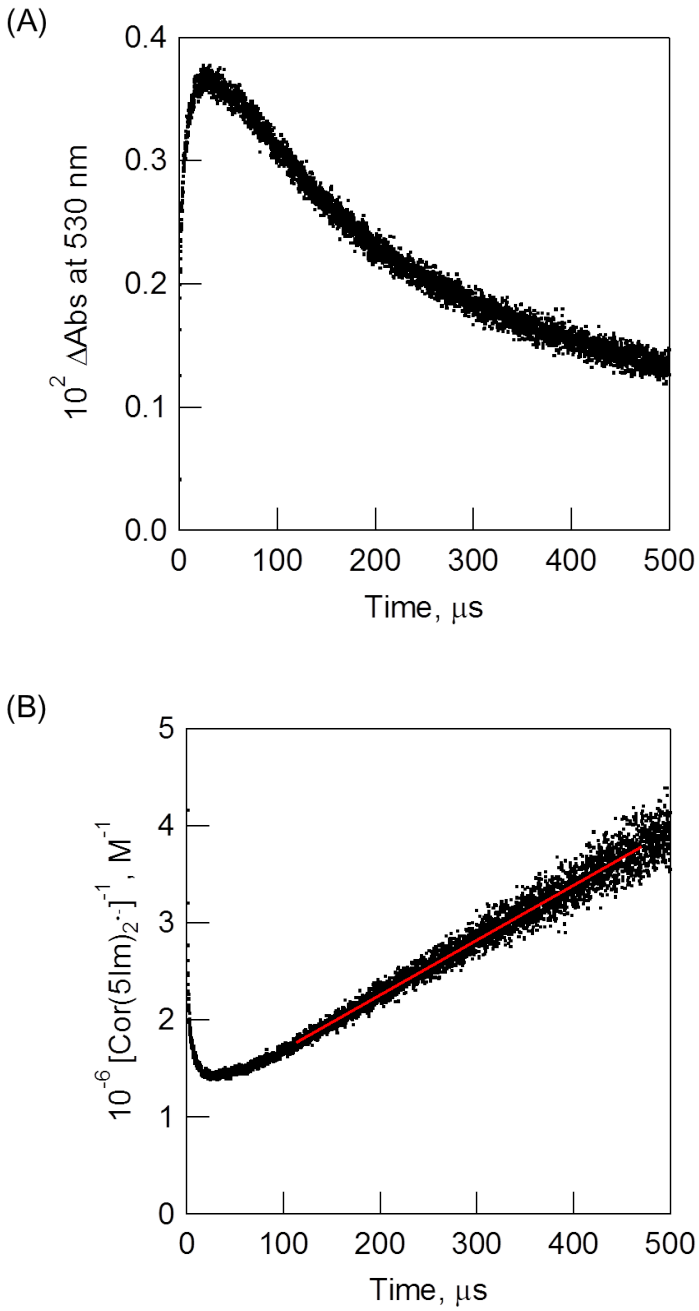

Figure S28. (A) Time profile of absorbance at 530 nm due to $Cor(5Im)_2^{\bullet-}$ upon nanosecond laser excitation to $Cor(5Im)_2$ (80 μM) and TPA (400 μM) in Ar-Saturated PhCN at 298 K. (B) The second-order plot of the decay of $Cor(5Im)_2^{\bullet-}$ obtained from the absorbance at 530 nm and the molar absorption coefficient ($\varepsilon = 5.2 \times 10^3$ M^{-1} cm^{-1}).

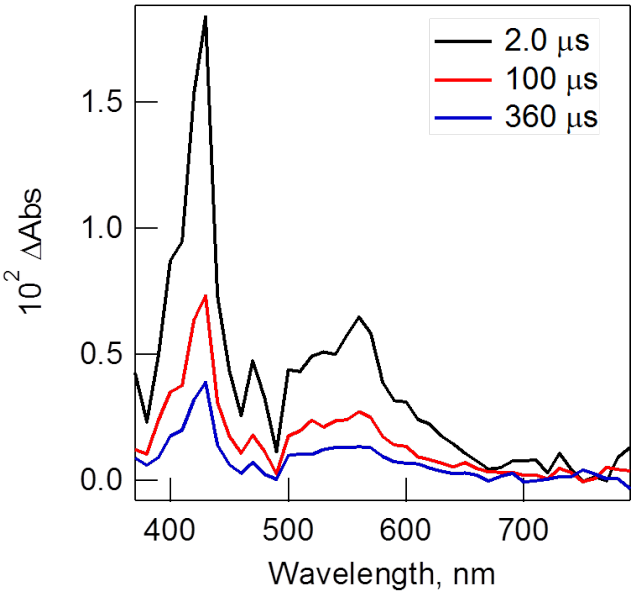

Figure S29. Transient absorption spectra of $Cor(5Im)_2$ (57 μM) in the presence of DMA (21 μM) in Ar-Saturated PhCN taken at 2.0 μs (black), 100 μs (red), and 360 μs (blue) after laser excitation at 355 nm at 298 K.

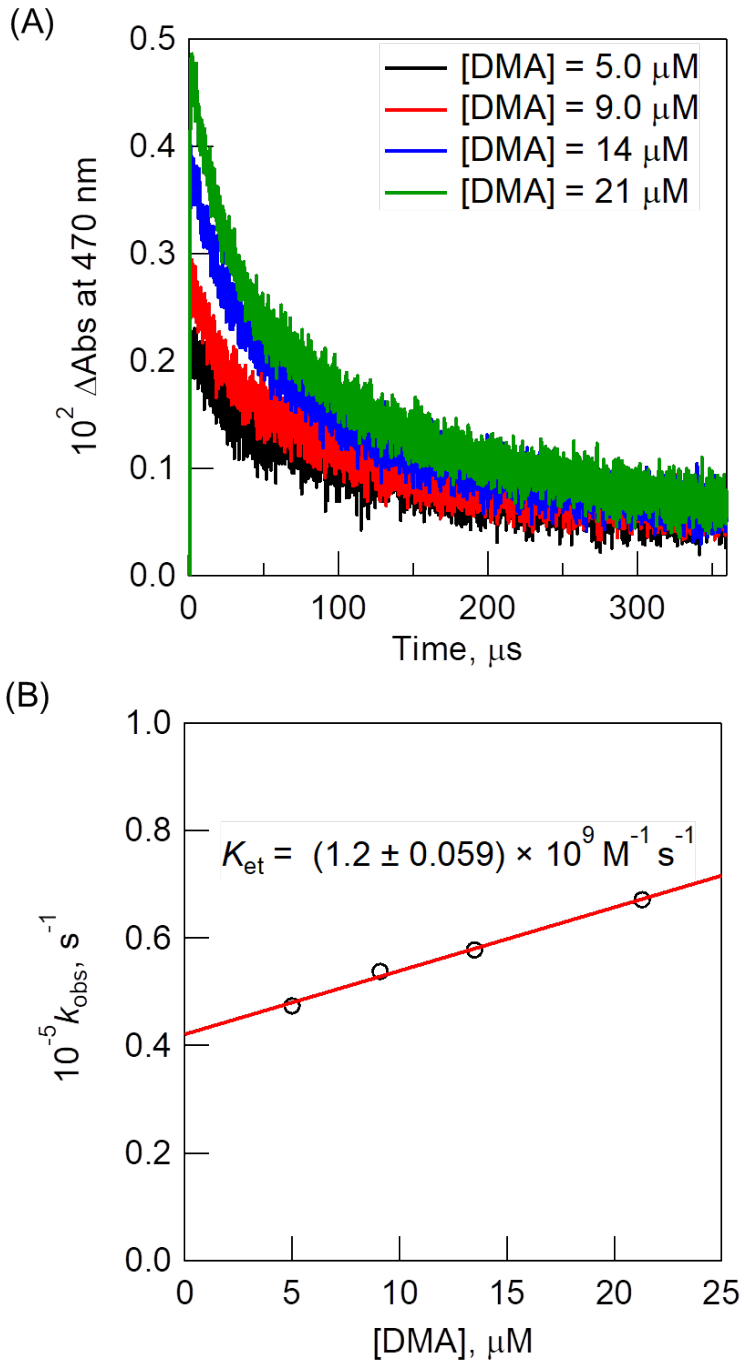

Figure S30. (A) Time profiles of absorbance at 470 nm due to $^{3}Cor(5Im)_2^{*}$ upon nanosecond laser excitation to $Cor(5Im)_2$ (78 μM) in the presence of varying concentrations of DMA in Ar-Saturated PhCN at 298 K. (B) Plot of the pseudo-first-order rate constant (k_{obs}) vs the concentration of DMA.

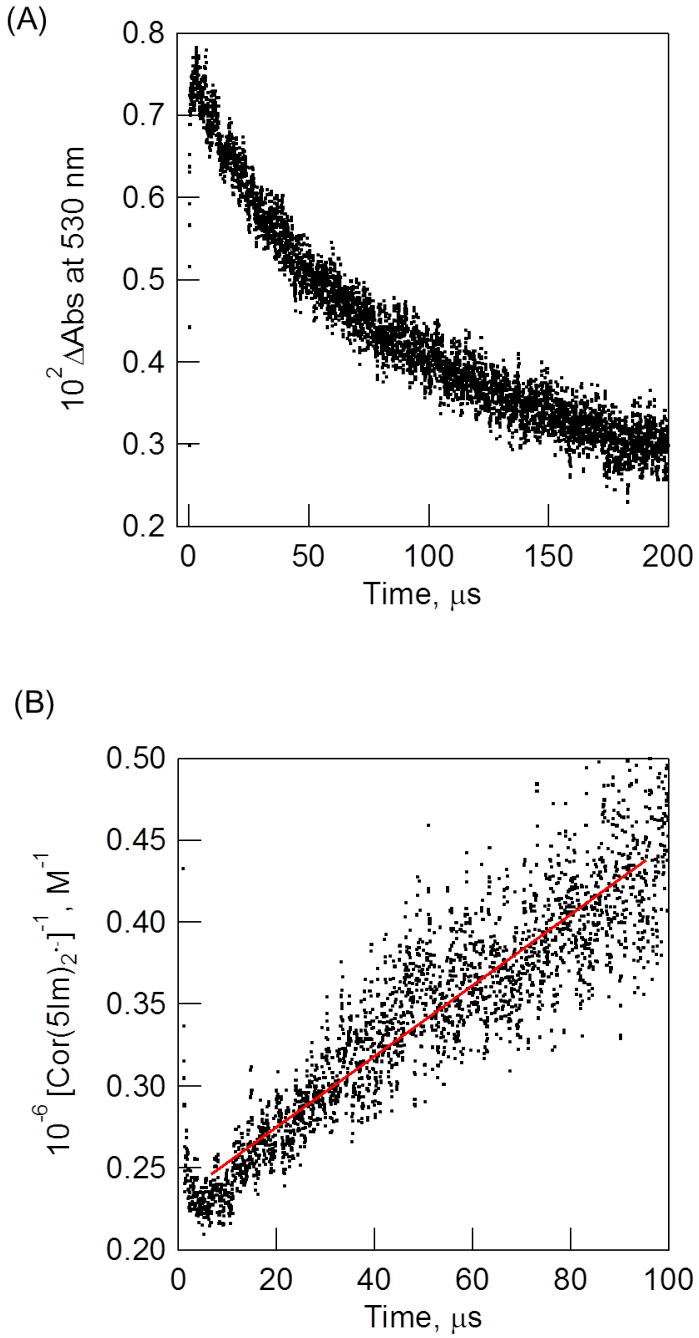

Figure S31. (A) Time profile of absorbance at 530 nm due to $Cor(5Im)_2^{\bullet-}$ upon nanosecond laser excitation to $Cor(5Im)_2$ (90 μM) and DMA (100 μM) in Ar-Saturated PhCN at 298 K. (B) The second-order plot of the decay of $Cor(5Im)_2^{\bullet-}$ obtained from the absorbance at 530 nm and the molar absorption coefficient ($\varepsilon = 5.2 \times 10^3$ M^{-1} cm^{-1}).

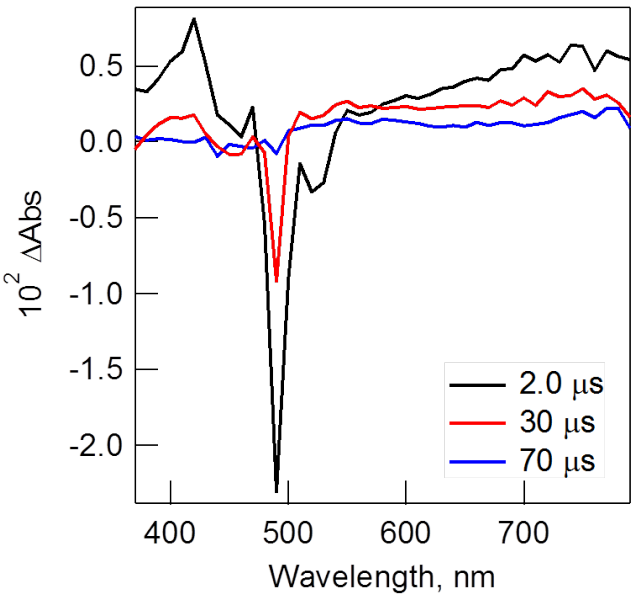

Figure S32. Transient absorption spectra of Cor(5Im)$_2$ (81 μM) in the presence of Pery (10 μM) in Ar-Saturated PhCN taken at 2.0 μs (black), 30 μs (red), and 70 μs (blue) after laser excitation at 298 K.

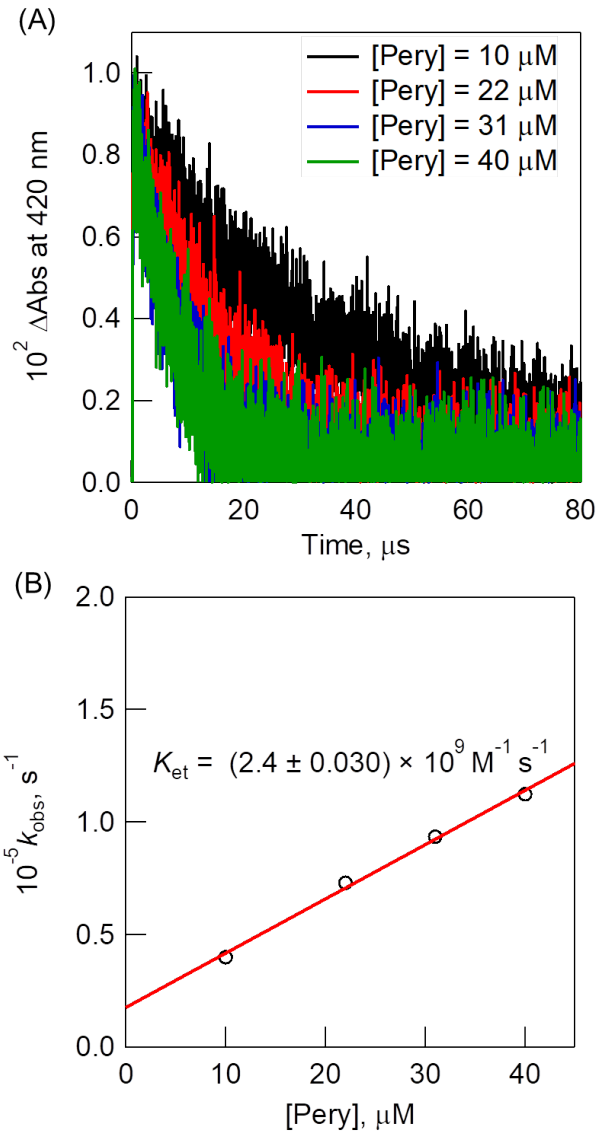

Figure S33. (A) Time profiles of absorbance at 420 nm due to $^{3}Cor(5Im)_2^{*}$ upon nanosecond laser excitation to $Cor(5Im)_2$ (66 μM) in the presence of varying concentrations of Pery in Ar-Saturated PhCN at 298 K. (B) Plot of the pseudo-first-order rate constant (k_{obs}) vs the concentration of Pery.

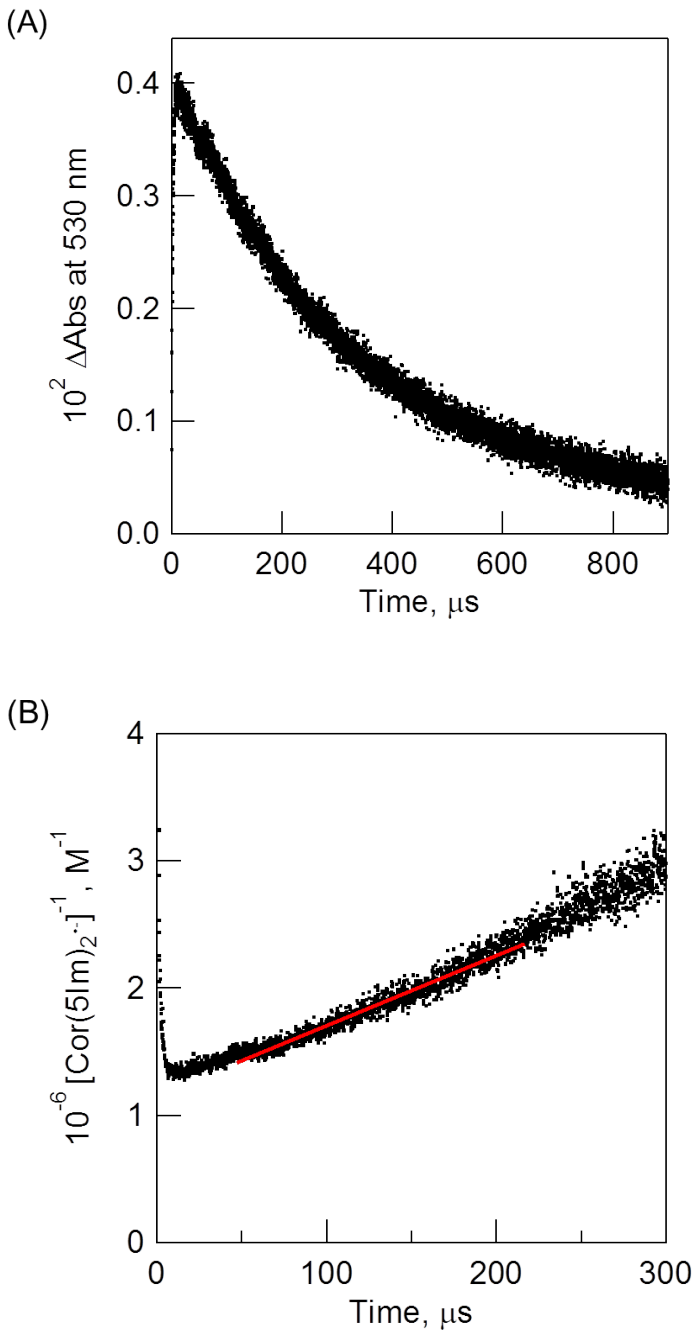

Figure S34. (A) Time profile of absorbance at 530 nm due to $Cor(5Im)_2^{\bullet-}$ upon nanosecond laser excitation to $Cor(5Im)_2$ (23 μM) and Pery (250 μM) in Ar-Saturated PhCN at 298 K. (B) The second-order plot of the decay of $Cor(5Im)_2^{\bullet-}$ obtained from the absorbance at 530 nm and the molar absorption coefficient ($\varepsilon = 5.2 \times 10^3$ M^{-1} cm^{-1}).

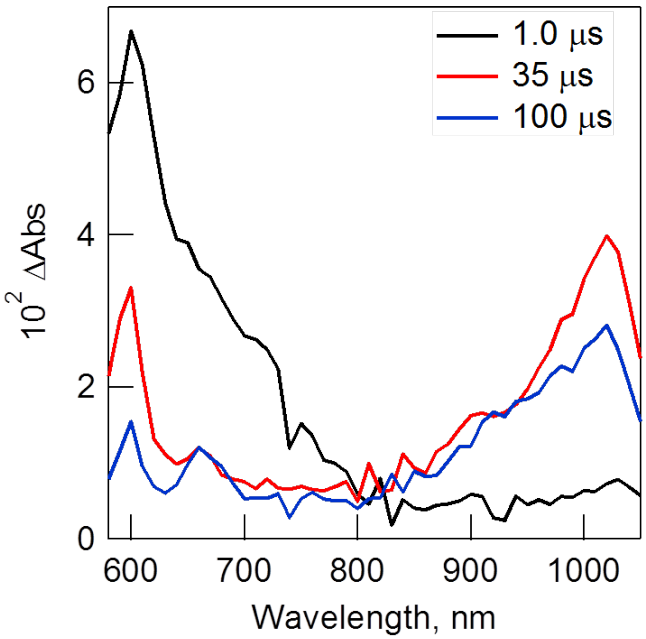

Figure S35. Transient absorption spectra of Cor(6Im)$_2$ (90 μM) in the presence of 2MI (100 μM) in Ar-Saturated PhCN taken at 1.0 μs (black), 35 μs (red), and 100 μs (blue) after laser excitation at 355 nm at 298 K.

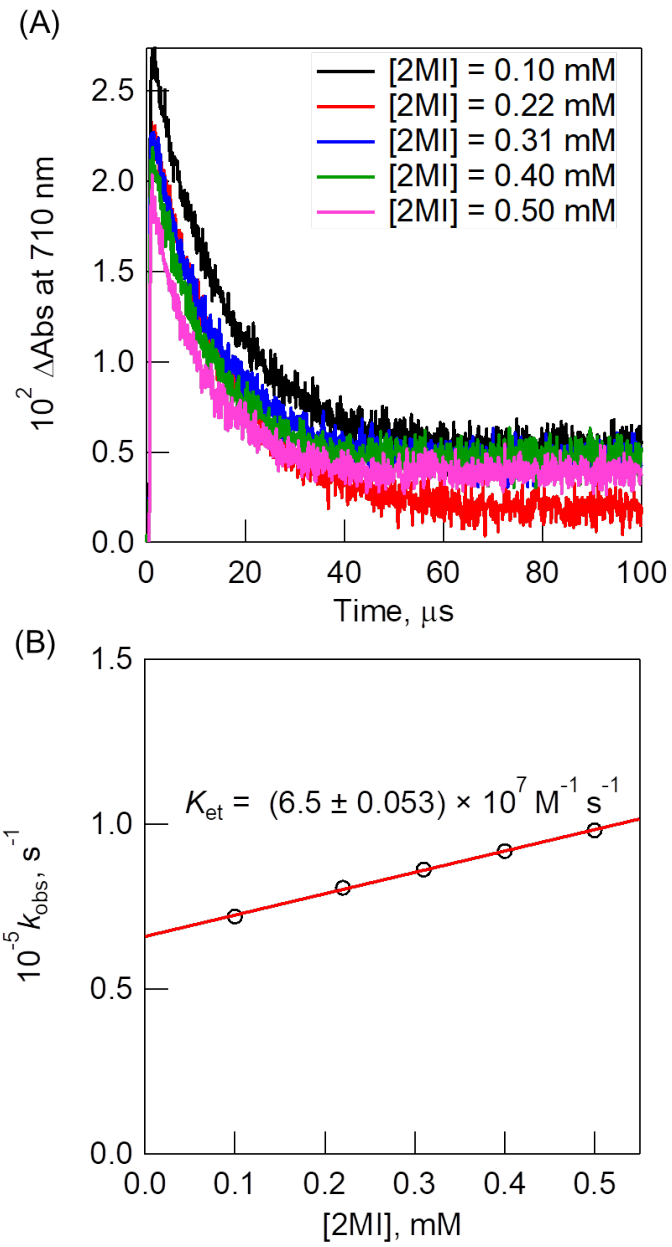

Figure S36. (A) Time profiles of absorbance at 710 nm due to $^{3}Cor(6Im)_2^{*}$ upon nanosecond laser excitation to $Cor(6Im)_2$ (69 μM) in the presence of varying concentrations of 2MI in Ar-Saturated PhCN at 298 K. (B) Plot of the pseudo-first-order rate constant (k_{obs}) vs the concentration of 2MI.

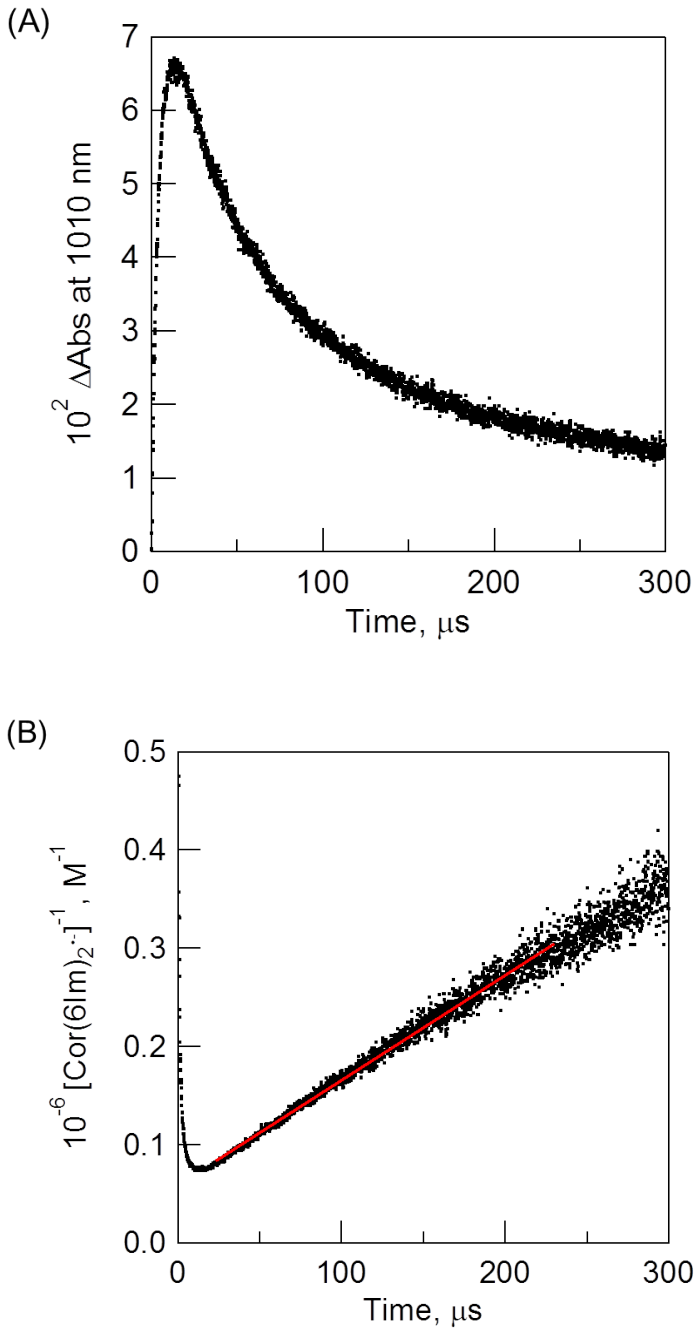

Figure S37. (A) Time profile of absorbance at 1010 nm due to $Cor(6Im)_2^{\bullet-}$ upon nanosecond laser excitation to $Cor(6Im)_2$ (90 μM) and 2MI (1.0 mM) in Ar-Saturated PhCN at 298 K. (B) The second-order plot of the decay of $Cor(6Im)_2^{\bullet-}$ obtained from the absorbance at 1010 nm and the molar absorption coefficient ($\varepsilon = 4.9 \times 10^3$ M^{-1} cm^{-1}).

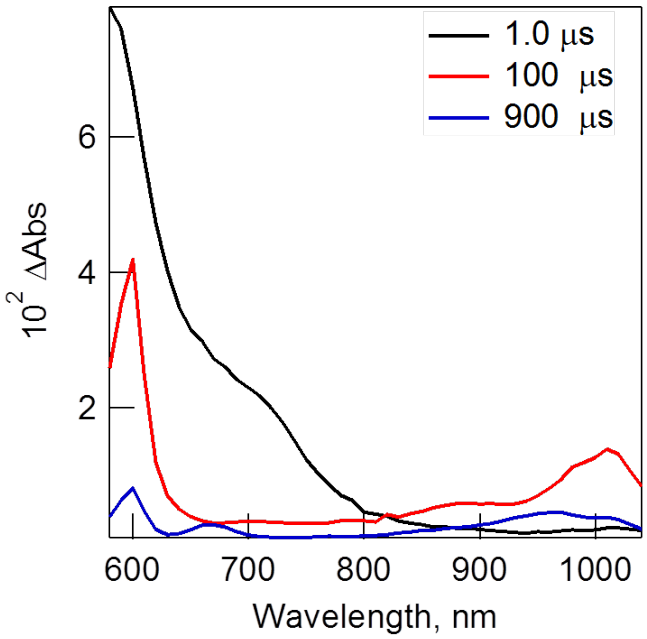

Figure S38. Transient absorption spectra of $Cor(6Im)_2$ (69 μM) in the presence of TEA (31 μM) in Ar-Saturated PhCN taken at 1.0 μs (black), 100 μs (red), and 900 μs (blue) after laser excitation at 355 nm at 298 K.

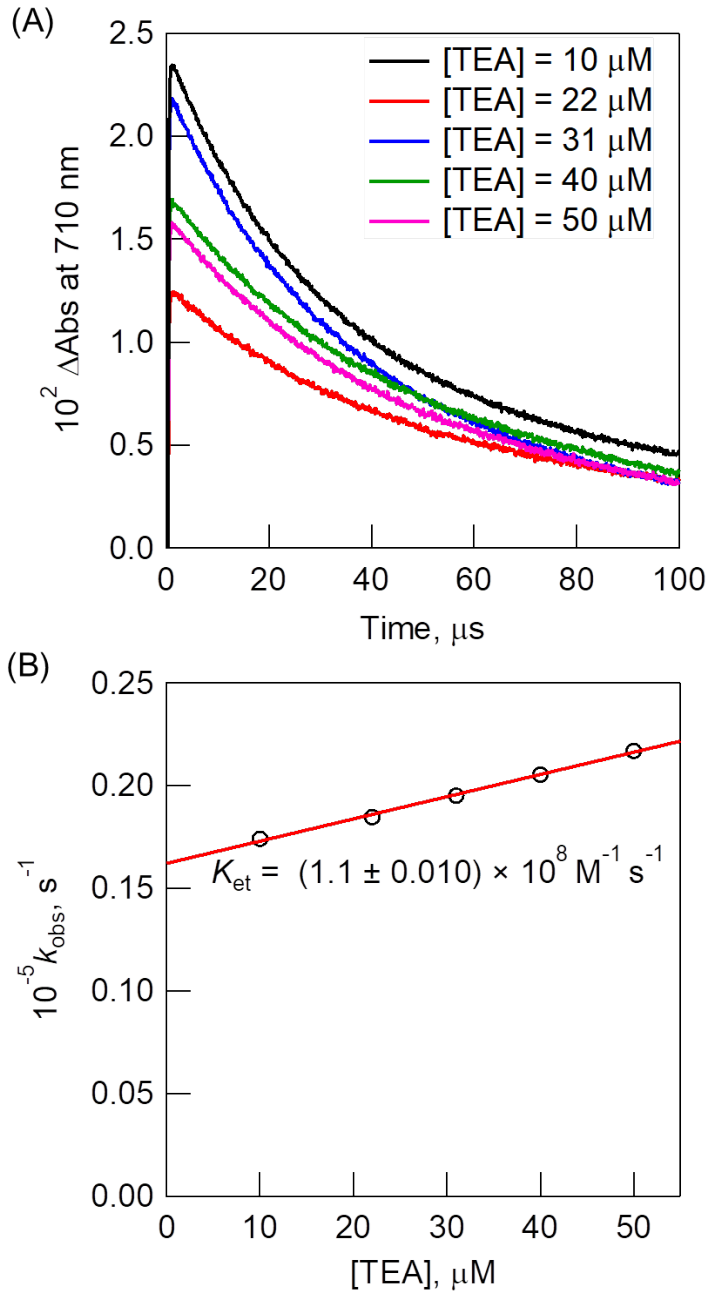

Figure S39. (A) Time profiles of absorbance at 710 nm due to $^{3}Cor(6Im)_2^{*}$ upon nanosecond laser excitation to $Cor(6Im)_2$ (69 μM) in the presence of varying concentrations of TEA in Ar-Saturated PhCN at 298 K. (B) Plot of the pseudo-first-order rate constant (k_{obs}) vs the concentration of TEA.

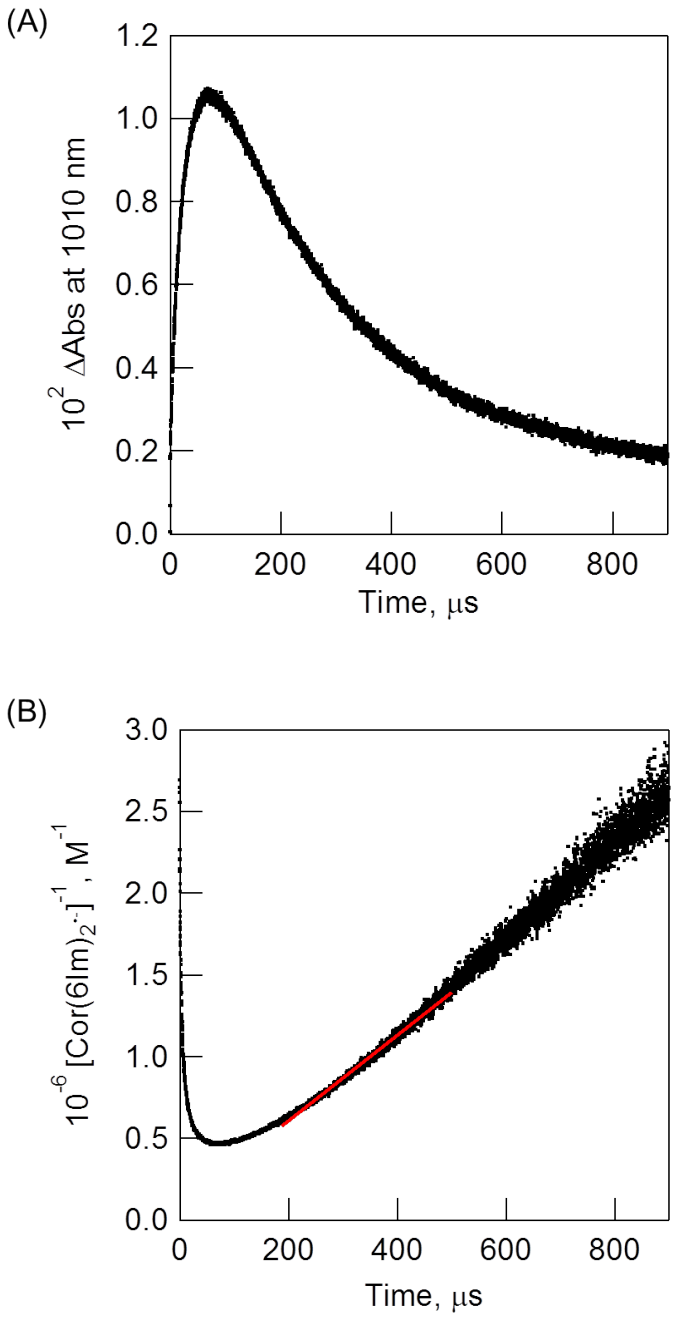

Figure S40. (A) Time profile of absorbance at 1010 nm due to $Cor(6Im)_2^{\bullet-}$ upon nanosecond laser excitation to $Cor(6Im)_2$ (90 μM) and TEA (10 μM) in Ar-Saturated PhCN at 298 K. (B) The second-order plot of the decay of $Cor(6Im)_2^{\bullet-}$ obtained from the absorbance at 1010 nm and the molar absorption coefficient ($\varepsilon = 4.9 \times 10^3$ M^{-1} cm^{-1}).

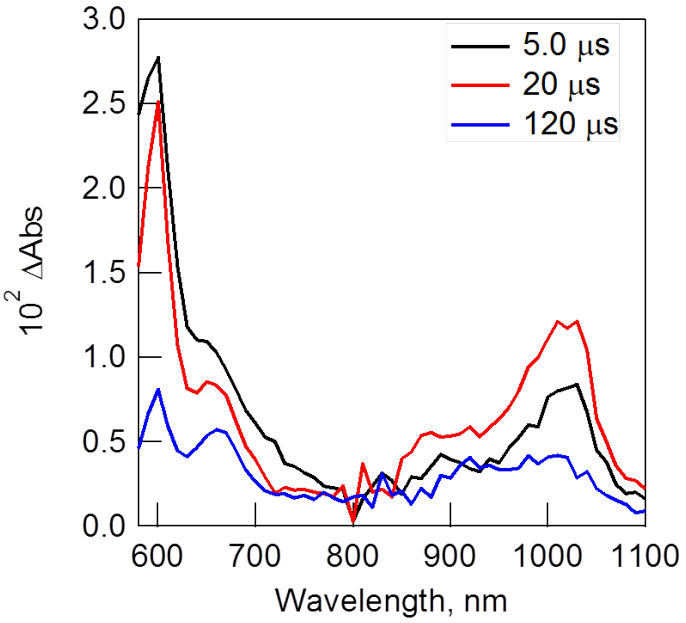

Figure S41. Transient absorption spectra of $Cor(6Im)_2$ (60 μM) in the presence of TPA (40 μM) in Ar-Saturated PhCN taken at 5.0 μs (black), 20 μs (red), and 120 μs (blue) after laser excitation at 355 nm at 298 K.

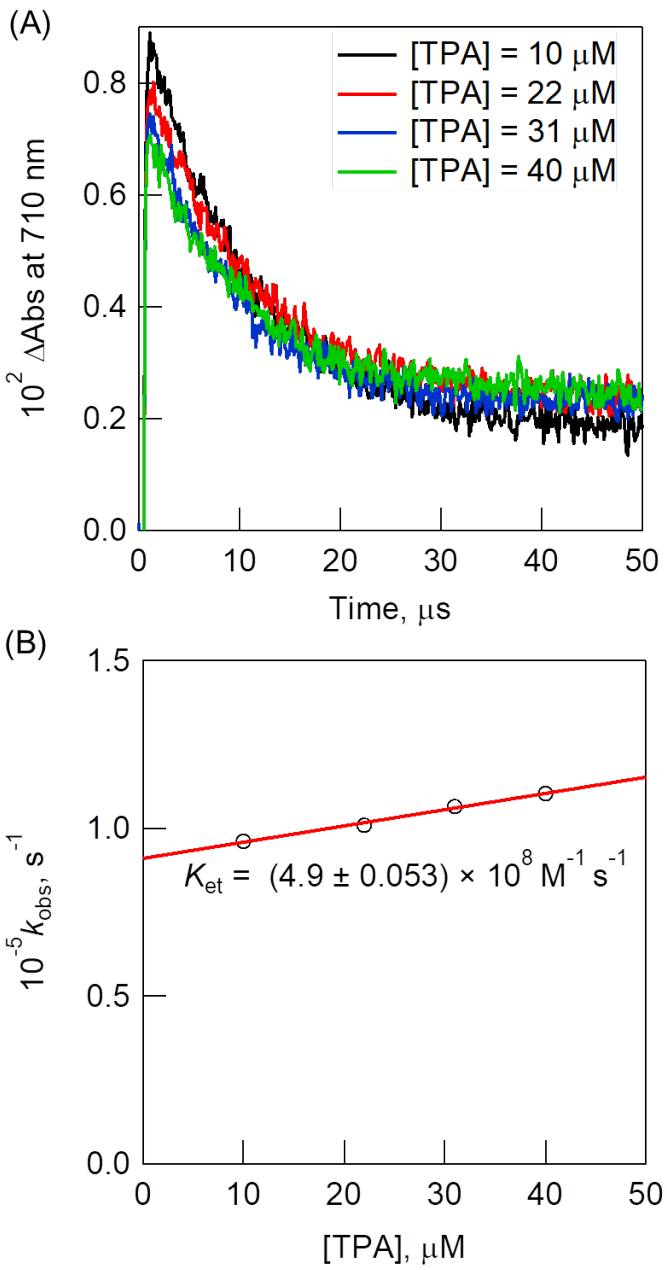

Figure S42. (A) Time profiles of absorbance at 710 nm due to $^{3}Cor(6Im)_2^{*}$ upon nanosecond laser excitation to $Cor(6Im)_2$ (74 μM) in the presence of varying concentrations of TPA in Ar-Saturated PhCN at 298 K. (B) Plot of the pseudo-first-order rate constant (k_{obs}) vs the concentration of TPA.

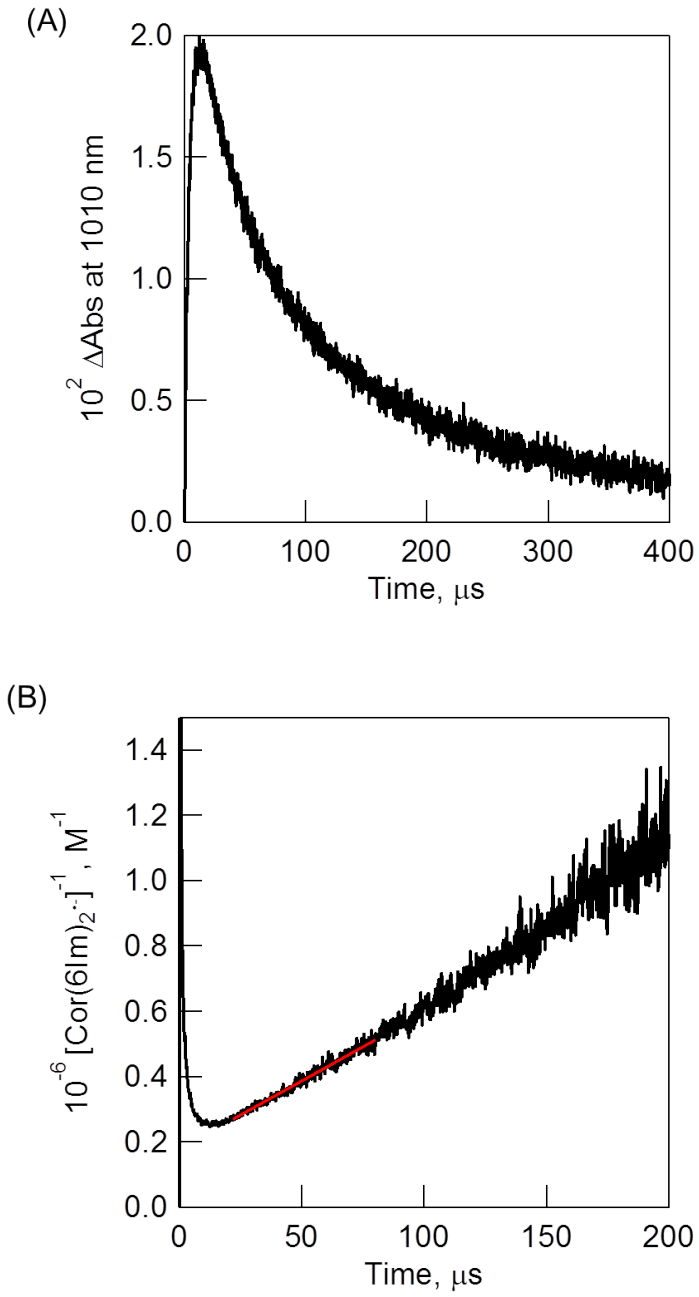

Figure S43. (A) Time profile of absorbance at 1010 nm due to $Cor(6Im)_2^{\bullet-}$ upon nanosecond laser excitation to $Cor(6Im)_2$ (90 μM) and TPA (100 μM) in Ar-Saturated PhCN at 298 K. (B) The second-order plot of the decay of $Cor(6Im)_2^{\bullet-}$ obtained from the absorbance at 1010 nm and the molar absorption coefficient ($\varepsilon = 4.9 \times 10^3$ M^{-1} cm^{-1}).

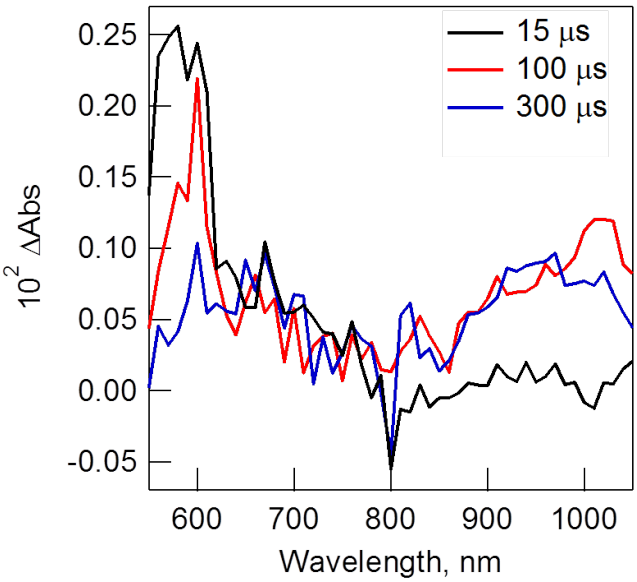

Figure S44. Transient absorption spectra of Cor(6Im)$_2$ (67 μM) in the presence of DMA (10 μM) in Ar-Saturated PhCN taken at 15 μs (black), 100 μs (red), and 300 μs (blue) after laser excitation at 355 nm at 298 K.

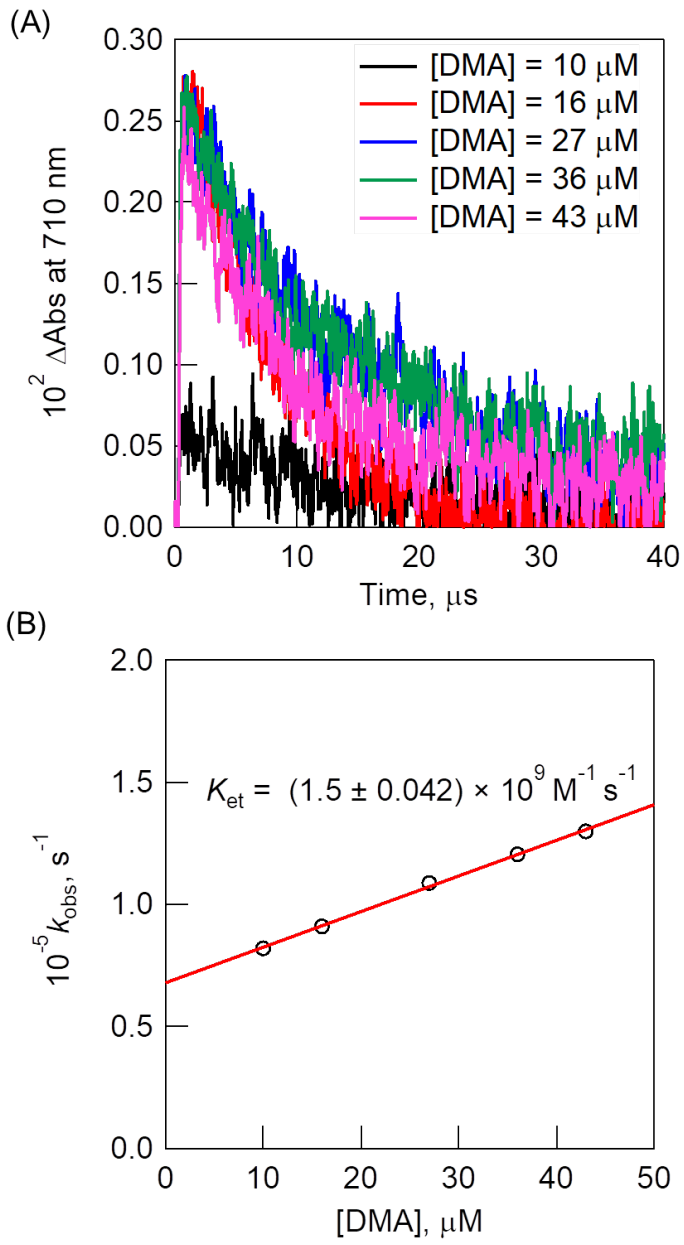

Figure S45. (A) Time profiles of absorbance at 710 nm due to $^{3}Cor(6Im)_2^{*}$ upon nanosecond laser excitation to $Cor(6Im)_2$ (54 μM) in the presence of varying concentrations of DMA in Ar-Saturated PhCN at 298 K. (B) Plot of the pseudo-first-order rate constant (k_{obs}) vs the concentration of DMA.

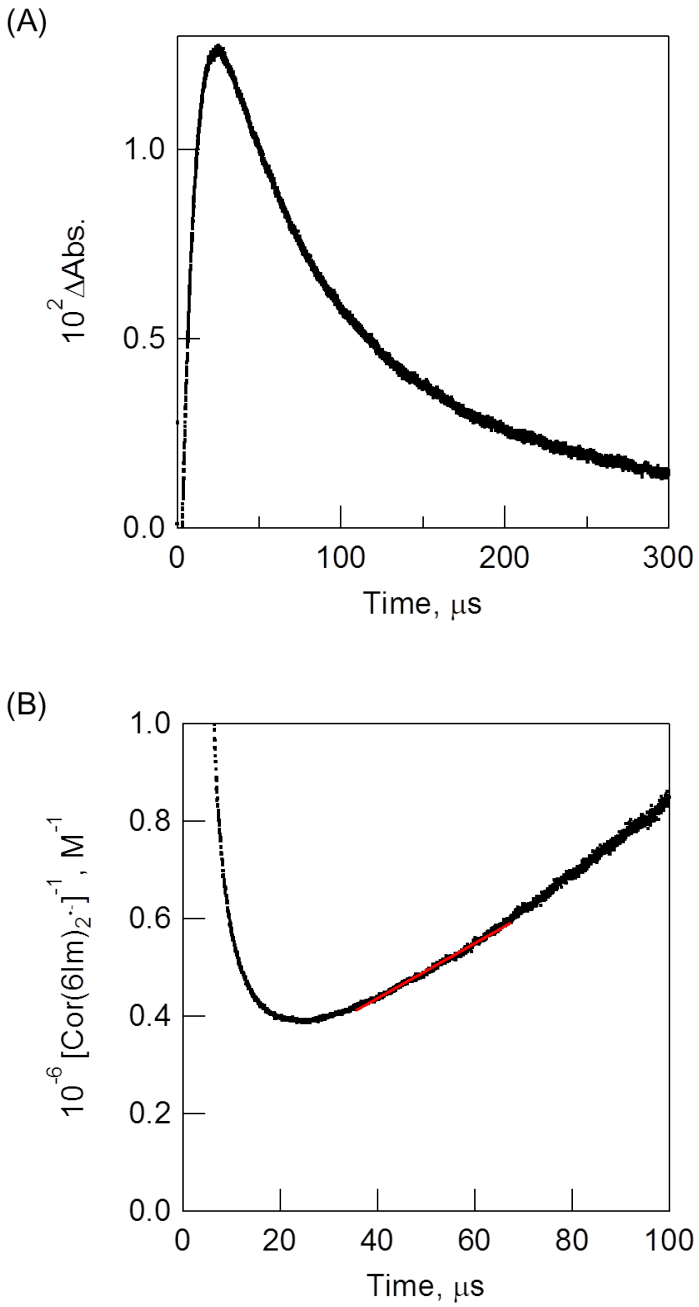

Figure S46. (A) Time profile of absorbance at 1010 nm due to $Cor(6Im)_2^{\bullet-}$ upon nanosecond laser excitation to $Cor(6Im)_2$ (70 μM) and DMA (500 μM) in Ar-Saturated PhCN at 298 K. (B) The second-order plot of the decay of $Cor(6Im)_2^{\bullet-}$ obtained from the absorbance at 1010 nm and the molar absorption coefficient ($\varepsilon = 4.9 \times 10^3$ M^{-1} cm^{-1}).

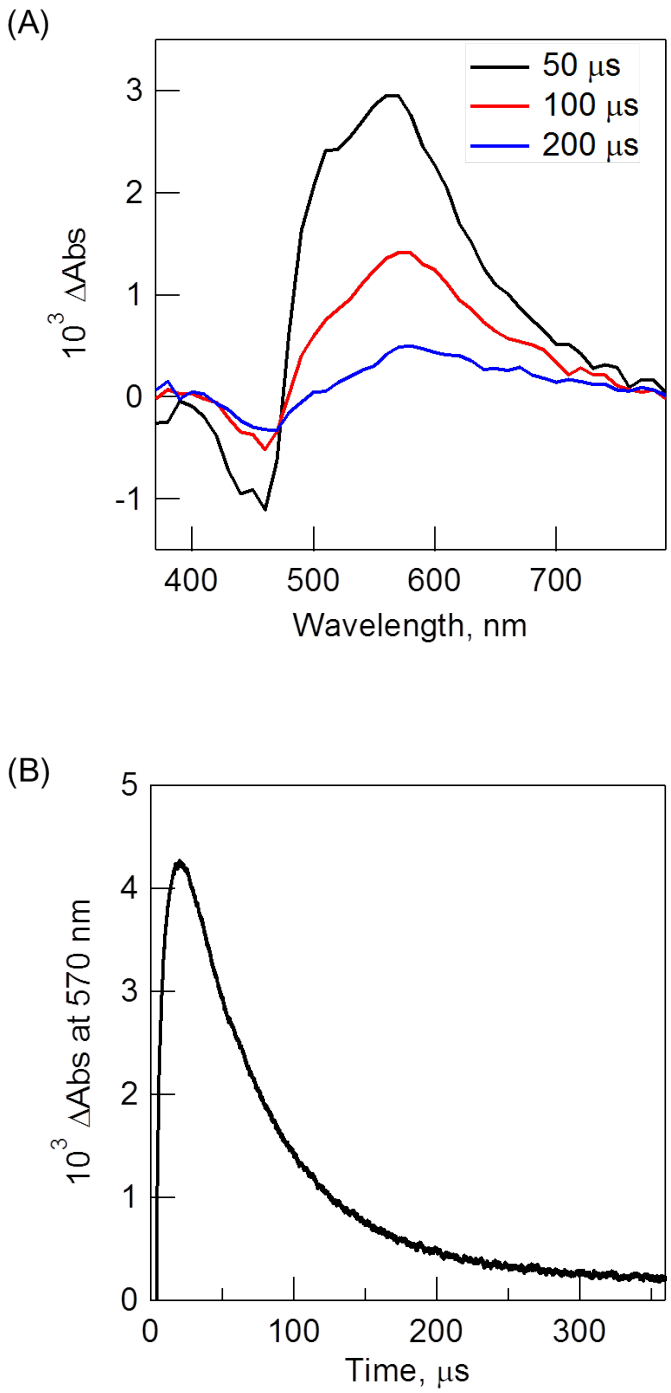

Figure S47. (A) Nanosecond transient absorption spectra of Pery (50 μM) in the presence of anthracene (50 μM) in Ar-Saturated PhCN taken at 50 μs (black), 100 μs (red), and 200 μs (blue) after laser excitation at 355 nm. (B) The time profile of absorbance at 570 nm.

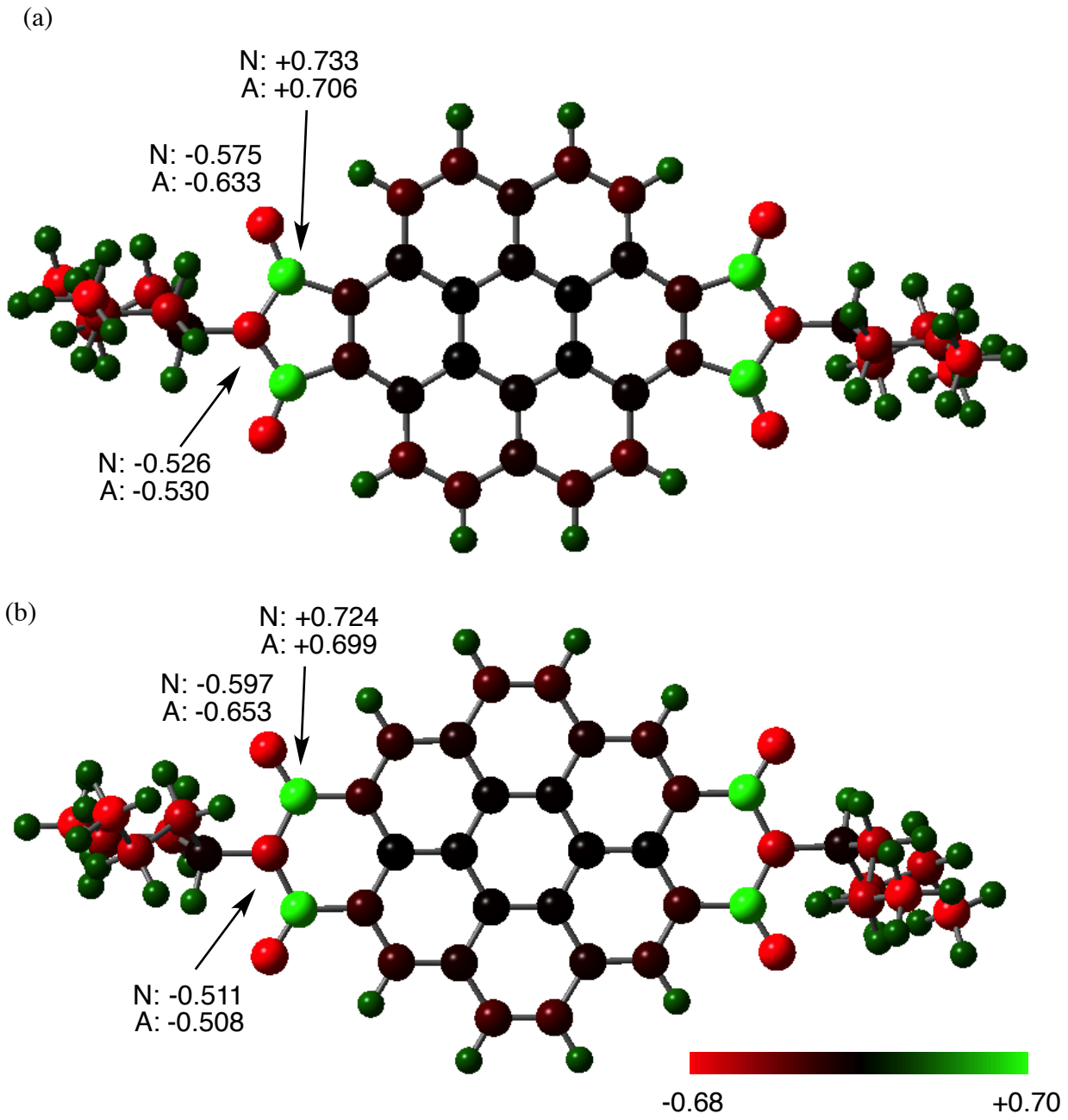

Figure S48. Charge density map of radical anions (a) $Cor(5Im)_2$ and (b) $Cor(6Im)_2$ calculated by natural population analyses (NPA) at the M06-2X/6-311+G(d,p) level of theory. Values are atomic charges of neutral and radical anion states.

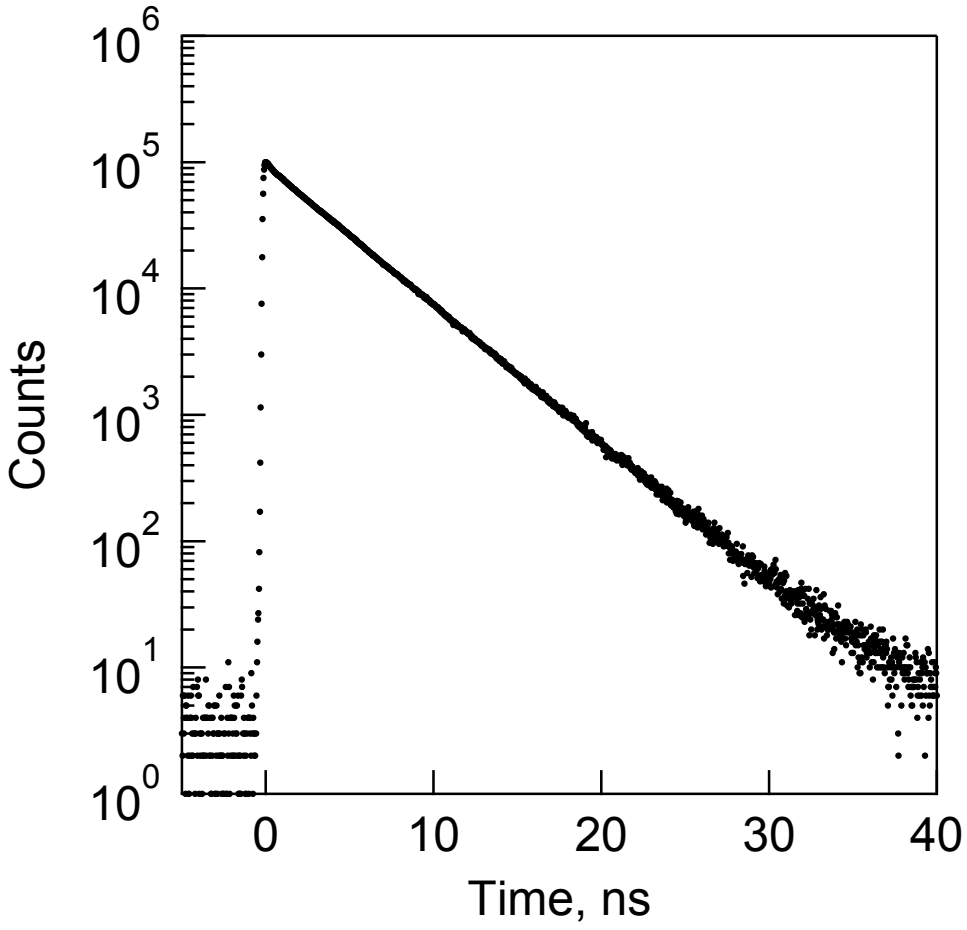

Figure S49. Fluorescence lifetime profile of Pery (20 μM) in Ar-Saturated PhCN. Excitation wavelength: 404 nm. The lifetime is ~ 3ns.